



HAL
open science

Atmospheric measurements of gas-phase HNO₃ and SO₂ using chemical ionization mass spectrometry during the MINATROC field campaign 2000 on Monte Cimone

M. Hanke, B. Umann, J. Uecker, F. Arnold, B. Bunz

► **To cite this version:**

M. Hanke, B. Umann, J. Uecker, F. Arnold, B. Bunz. Atmospheric measurements of gas-phase HNO₃ and SO₂ using chemical ionization mass spectrometry during the MINATROC field campaign 2000 on Monte Cimone. *Atmospheric Chemistry and Physics Discussions*, 2002, 2 (6), pp.2209-2258. hal-00300997

HAL Id: hal-00300997

<https://hal.science/hal-00300997>

Submitted on 18 Jun 2008

HAL is a multi-disciplinary open access archive for the deposit and dissemination of scientific research documents, whether they are published or not. The documents may come from teaching and research institutions in France or abroad, or from public or private research centers.

L'archive ouverte pluridisciplinaire **HAL**, est destinée au dépôt et à la diffusion de documents scientifiques de niveau recherche, publiés ou non, émanant des établissements d'enseignement et de recherche français ou étrangers, des laboratoires publics ou privés.

**Atmospheric
measurements of
gas-phase HNO₃
and SO₂**

M. Hanke et al.

Atmospheric measurements of gas-phase HNO₃ and SO₂ using chemical ionization mass spectrometry during the MINATROC field campaign 2000 on Monte Cimone

M. Hanke¹, B. Umann¹, J. Uecker¹, F. Arnold¹, and H. Bunz²

¹Atmospheric Physics Division, Max-Planck-Institut für Kernphysik, Heidelberg, Germany

²Atmospheric Aerosol Research Department, Institute of Meteorology and Climate Research, Forschungszentrum Karlsruhe, Germany

Received: 18 September 2002 – Accepted: 11 November 2002 – Published:
28 November 2002

Correspondence to: Markus Hanke (markus.hanke@mpi-hd.mpg.de)

Title Page

Abstract

Introduction

Conclusions

References

Tables

Figures

⏪

⏩

◀

▶

Back

Close

Full Screen / Esc

Print Version

Interactive Discussion

Abstract

The EU-project MINATROC (MINeral dust And TROpospheric Chemistry) aims at enabling an estimation of the influence of mineral dust, a major, but to date largely ignored component of tropospheric aerosol, on tropospheric oxidant cycles. Within the scope of this project continuous atmospheric measurements of gas-phase HNO_3 and SO_2 were conducted in June and July 2000 at the CNR WMO station, situated on Monte Cimone (MTC) ($44^\circ 11' \text{ N} - 10^\circ 42' \text{ E}$, 2165 m asl), Italy. African air transporting dust is occasionally advected over the Mediterranean Sea to the site, thus mineral aerosol emitted from Africa will encounter polluted air masses and provide ideal conditions to study their interactions. HNO_3 and SO_2 were measured with an improved CIMS (chemical ionization mass spectrometry) system for ground-based measurements that was developed and built at MPI-K Heidelberg. Since HNO_3 is a very sticky compound special care was paid for the air-sampling and background-measurement system. Complete data sets could be obtained before, during and after major dust intrusions. For the first time these measurements might provide a strong observational indication of efficient uptake of gas-phase HNO_3 by atmospheric mineral-dust aerosol particles.

1. Introduction

Gaseous nitric acid (HNO_3) is one of the most important acidic air pollutants reaching typical mixing ratios of the order of several parts per billion by volume (ppbv) in polluted air and a few tens of parts per trillion by volume (pptv) in clean air (Goldan et al., 1984). It represents an important component of the NO_y family in the troposphere. The association reaction of OH radicals with NO_2 constitutes the primary source of HNO_3 in the troposphere during the day. At night the heterogeneous hydrolysis of dinitrogen pentoxide, N_2O_5 , and reactions of the nitrate radical, NO_3 , are likely to account for most of the HNO_3 formation (Dentener et al., 1993). HNO_3 is relatively unreactive in the gas phase with chemical and photochemical lifetimes of 2 and several weeks, respectively

Atmospheric measurements of gas-phase HNO_3 and SO_2

M. Hanke et al.

Title Page

Abstract

Introduction

Conclusions

References

Tables

Figures

◀

▶

◀

▶

Back

Close

Full Screen / Esc

Print Version

Interactive Discussion

**Atmospheric
measurements of
gas-phase HNO₃
and SO₂**

M. Hanke et al.

Title Page

Abstract

Introduction

Conclusions

References

Tables

Figures

◀

▶

◀

▶

Back

Close

Full Screen / Esc

Print Version

Interactive Discussion

(Kley et al., 1981; Liu et al., 1987). Once formed, HNO₃ can be efficiently removed on a time scale of a few days by rain-out and surface deposition (Parrish et al., 1986; Liu et al., 1983). In the upper troposphere, where the heterogeneous loss processes are not that effective anymore and the photolysis of HNO₃ becomes more important, HNO₃ can act as an important reservoir for NO_x. This highly affects the O₃ concentration in the upper troposphere (Tabazadeh et al., 1998).

Sulfur dioxide (SO₂), the predominant anthropogenic sulfur-containing air pollutant reaching mixing ratios of the order of 10 ppbv and more in urban areas and less than 10 pptv in remote regions (Seinfeld and Pandis, 1997), originates in the troposphere of the Northern Hemisphere mostly from direct anthropogenic emissions (fossil fuel burning). Secondary oxidation following the release of reduced sulfur compounds by natural metabolism processes or volcanic emissions (Berresheim and Jaeschke, 1983; Berresheim 1995) are of minor importance for continental air masses of the Northern Hemisphere. SO₂ is efficiently removed from the atmosphere by dry and wet deposition. The dominant removal pathway of SO₂ in the atmosphere, however, is believed to be the oxidation to sulfate either in the gas phase or in aqueous phase and thus promoting aerosol and cloud formation. The average lifetime of SO₂ is of the order of one day in the planetary boundary layer and up to about 15 days in the free troposphere. The conversion to sulfate is important because it changes the radiative effects of aerosols (IPCC 2001).

Only very recently mineral dust has attained increasing interest because of its role in the Earth's climate system. It may influence the radiative budget and the concentrations and lifetimes of many important atmospheric species by undergoing reactions with atmospheric gases or serving as carriers and/or sinks (e.g. Tegen and Fung, 1994, 1995; Dentener et al., 1996; Zhang et al., 1996; Phadnis and Carmichael, 2000). The overall impact exerted by heterogeneous reactions of SO₂, HNO₃, N₂O₅, HONO, NO₃, NO₂, H₂O₂, and HO₂ on mineral aerosol has been assessed in combined aerosol/gas-phase models, (e.g. Zhang et al., 1994; Dentener et al., 1996). For example in the modelling study of Dentener et al. (1996), it has been shown that an efficient interac-

**Atmospheric
measurements of
gas-phase HNO₃
and SO₂**

M. Hanke et al.

Title Page

Abstract

Introduction

Conclusions

References

Tables

Figures

◀

▶

◀

▶

Back

Close

Full Screen / Esc

Print Version

Interactive Discussion

tion of SO₂ with mineral aerosol can result in a substantial oxidation to sulfate at the surface of mineral aerosol in the troposphere. Mineral dust particles with a coating of sulfate have been observed by, e.g. Foner and Ganor (1992). Recent laboratory studies have shown the uptake of SO₂ on calcite (CaCO₃) surfaces using a low-pressure coated flow-tube reactor coupled to an electron-impact mass spectrometer (Adams et al., 2002). The above-mentioned model studies have also emphasized the importance of including the HNO₃/mineral particle interactions in tropospheric chemistry models. Observations by Galy-Lacaux and Modi (1998), in the Sahelian region during the wet season have demonstrated that the alkalinity of the dust particles favors the uptake of nitrogenous compounds, especially HNO₃. Laboratory studies of Goodman et al. (2000), have confirmed that HNO₃ removal by CaCO₃ particles could be significant in the atmosphere, as has been suggested by Dentener et al. (1996), and Tabazedeh et al. (1998). The importance of heterogeneous reactions of HNO₃ on mineral dust has been further supported by a combined laboratory and modeling study of Underwood et al. (2001), who have shown that under conditions of high mineral dust loadings and/or smaller size distributions the importance of these reactions is expected to increase. These observations and model calculations indicate that the presence of mineral dust can have a strong impact on aerosol formation and photochemical oxidant cycles in the troposphere. As possible consequences, the degree of mixing of sulfate or nitrate with mineral dust will affect the radiative and cloud activation properties of each of these compounds, and hence their effect on climate. Furthermore, processes that alter the NO_x to NO_y ratio (e.g. loss of gas-phase N₂O₅ or HNO₃ to mineral dust or recycling of NO_x from HNO₃ more efficiently than HNO₃ photolysis or reactions with OH), or HO_x concentrations (e.g. heterogeneous conversion of NO₂ to HONO) directly influence O₃ concentrations.

An accurate assessment of the role of mineral dust in tropospheric chemistry has not been possible due to the lack of observational data. A key uncertainty with regard to tropospheric observations and thus to address the above-mentioned issues concerns the capability of the current methods to adequately measure gas-phase HNO₃ and

SO₂ including also the lower pptv range with a good time resolution, sensitivity and reliability.

In particular techniques for reliable ground-based measurements of gas-phase HNO₃ are not well established and developed (Parrish et al., 2000). Intercomparison campaigns using different experimental methods for measuring gaseous HNO₃, including the filter-pack method, denuder-tube technique and tunable-diode-laser absorption method have found only relatively poor agreement between the different techniques even at relatively high HNO₃ levels and demonstrated that none of the techniques was capable of measuring HNO₃ below 100 pptv for integration times of less than 10 min (Gregory et al., 1990). Further methods, the mist chamber method of Talbot et al. (1990) and the laser-photolysis fragment-fluorescence method of Papenbrock and Stuhl (1990), reported detection limits of 10 and 100 pptv, respectively, for an integration time of 10 min. Recently novel HNO₃ measurement techniques, based on chemical ionization mass spectrometry (CIMS), have been developed to overcome the drawbacks of the other techniques (Arnold et al., 1985; Schneider et al., 1998; Huey et al., 1996; Mauldin et al., 1998; Miller et al., 2000; Furutani et al., 2002). All of these techniques show sensitivities to mixing ratios less than 50 pptv and integration times faster than 15 s. In an informal field intercomparison two different CIMS techniques were principally in good agreement (Fehsenfeld et al., 1998). A short review of these different methods for measuring gaseous HNO₃ is also given in Parrish and Fehsenfeld (2000).

Former intercomparison experiments have shown that measuring SO₂ down to the pptv levels also bears difficulties. For SO₂ of a few pptv to 200 pptv, the third Chemical Instrumentation and Testing Experiment (CITE 3), an intercomparison experiment of five different SO₂ methods ranging from filter techniques to near real-time measurements (chemiluminescent, GC-MS, GC-flame photometric) has shown that there was no general agreement among the techniques and the results from the instruments were uncorrelated (Gregory et al., 1993). More recently, with respect to ground-based measurements of atmospheric SO₂, seven techniques (aqueous chemiluminescence,

**Atmospheric
measurements of
gas-phase HNO₃
and SO₂**M. Hanke et al.

[Title Page](#)[Abstract](#)[Introduction](#)[Conclusions](#)[References](#)[Tables](#)[Figures](#)[⏪](#)[⏩](#)[◀](#)[▶](#)[Back](#)[Close](#)[Full Screen / Esc](#)[Print Version](#)[Interactive Discussion](#)

**Atmospheric
measurements of
gas-phase HNO₃
and SO₂**M. Hanke et al.

[Title Page](#)[Abstract](#)[Introduction](#)[Conclusions](#)[References](#)[Tables](#)[Figures](#)[⏪](#)[⏩](#)[◀](#)[▶](#)[Back](#)[Close](#)[Full Screen / Esc](#)[Print Version](#)[Interactive Discussion](#)

pulsed resonance fluorescence detection, isotope dilution-gas chromatography followed by mass spectrometric detection, mist chamber-ion chromatography, diffusion denuder with sulfur chemiluminescence detection (DD-SCD), high performance liquid chromatography with fluorescence detection, and carbonate filter with ion chromatographic detection) were compared simultaneously in the Gas-phase Sulfur Intercomparison Experiment (GAISE) in 1994 (Luther and Stecher, 1997; Stecher et al., 1997). This intercomparison already showed better results. Six of the seven techniques compared well even below 500 pptv, with good linear response and no serious interferences. The time resolutions were of the order of a few minutes to up to 90 min for the filter-IC. The intercomparison, however, showed, that there are no validated standards for low pptv concentrations. Also CIMS has proven to be a versatile and extremely sensitive technique for monitoring SO₂, in particular with regard to aircraft-borne measurements due to its sensitivity to mixing ratios less than 100 pptv and response times faster than 15 s. (Arnold et al., 1997; Hunton et al., 2000; Reiner et al., 2001).

The EU-funded project MINATROC (MINeral dust And TROpospheric Chemistry) is a concerted, multidisciplinary effort that combines laboratory work, field observations and model development and application. An overview of the goals of this project in general and the Monte Cimone experiment in particular is given in the paper of Balkanski et al., this issue. The first field campaign of MINATROC took place between May and July 2000 at the CNR WMO station, situated on Monte Cimone (MTC), the highest peak of the Northern Apennines (2165 m asl) in Italy (Bonasoni et al., 2000). The site was chosen because African air transporting dust is occasionally advected over the Mediterranean Sea to the site. Thus mineral aerosol emitted from Africa will encounter polluted air masses and provide ideal conditions to study their interactions, in particular to quantify the impact of mineral dust on tropospheric photochemical cycles leading to ozone production and destruction.

We participated in the field study with continuous measurements of gaseous HNO₃ and SO₂ with an improved CIMS instrument developed and built by MPI-K, based on the experience of previous aircraft-borne instruments (Arnold et al., 1985, 1997;

**Atmospheric
measurements of
gas-phase HNO₃
and SO₂**M. Hanke et al.

[Title Page](#)[Abstract](#)[Introduction](#)[Conclusions](#)[References](#)[Tables](#)[Figures](#)[◀](#)[▶](#)[◀](#)[▶](#)[Back](#)[Close](#)[Full Screen / Esc](#)[Print Version](#)[Interactive Discussion](#)

Schneider et al., 1998). In particular this instrument was designed to meet the requirements for fast, reliable and continuous sensitive ground-based measurements of these species in the boundary layer and lower free troposphere, i.e. atmospheric conditions typically encountered on MTC, where rather high relative humidities are frequent. Due to the specific sticky character of HNO₃ special care was paid to the air-sampling and background-measurement system. The instrument was automated in such a way that continuous measurements of HNO₃ and SO₂ could be carried out during the campaign.

Further measurements of NO, NO₂, NO_y, O₃, HCHO, CO, VOCs, CO₂, sum of RO₂, J(O¹D), aerosol, and meteorological parameters were performed (Fischer et al., this issue, Bonasoni et al., this issue, Van Dingenen et al., this issue). In addition speciated measurements of HO₂ and RO₂ with the CIMS-based ROxMAS technique of MPI-K (Hanke et al., this issue, Hanke et al., 2002), were carried out.

In this paper we will first describe our improved CIMS instrument before we report on the atmospheric measurements of HNO₃ and SO₂ during the MINATROC field campaign. Measurements during a major dust intrusion between 3 and 4 July 2000 might provide, for the first time, a strong observational indication of efficient uptake of gaseous HNO₃ by atmospheric mineral dust aerosol particles.

2. Experimental section

2.1. CIMS apparatus

For the MINATROC 2000 field campaign on Monte Cimone, a new CIMS apparatus for ground-based measurements of HNO₃ and SO₂ has been developed, built and tested in our laboratory of MPI-K, Heidelberg, before it was deployed on Monte Cimone. The principle of the MPI-K CIMS technique, which has been originally developed for atmospheric applications on rockets, balloons, and aircraft, has been described by, e.g. Arnold and Hauck (1985), Arnold et al. (1997), Knop and Arnold (1985, 1987), Möhler and Arnold (1991), Möhler et al. (1993) and Schneider et al. (1998).

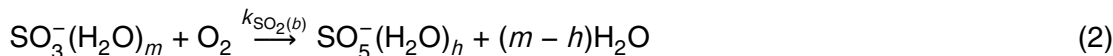
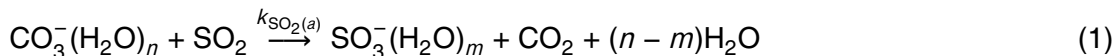
Atmospheric measurements of gas-phase HNO₃ and SO₂

M. Hanke et al.

[Title Page](#)
[Abstract](#)
[Introduction](#)
[Conclusions](#)
[References](#)
[Tables](#)
[Figures](#)
[⏪](#)
[⏩](#)
[◀](#)
[▶](#)
[Back](#)
[Close](#)
[Full Screen / Esc](#)
[Print Version](#)
[Interactive Discussion](#)

For the ground-based deployment special care was paid to air sampling, calibration, and background measurements as will be discussed below. Furthermore, the instrument was automated in such a way that continuous long-term measurements of SO₂ and HNO₃ could be carried out.

A schematic diagram of the CIMS apparatus is shown in Fig. 1. The main components of the instrument are a heated PFA Teflon sampling system (see discussion below), a stainless-steel flow-tube reactor (FR) with a tubular inlay made of Teflon (3.3 cm inner diameter ID, thermostatted at ~40°C), a gas-discharge ion source, and a quadrupole mass spectrometer. In the sampling line and FR a pressure of about 50 mbar is maintained by an oil-free 30 m³/h SCROLL pump. Due to the pressure gradient between the FR and the atmosphere (usually around 790 mbar), ambient air is drawn at a flow rate of about (12.4 ± 0.5) slm (= L/min at standard temperature and pressure) through a (1.35 ± 0.05) mm diameter heated PFA orifice and then through the 1/2 inch (outer diameter, 9.3 mm ID) heated PFA Teflon sampling tube into the left end of the flow-tube reactor (see Fig. 1). At a distance of 17 cm downstream CO₃⁻ ions are injected into the FR. The ionization is spatially separated from the main gas flow by a capillary tube, through which a source gas, composed of 1.4 slm O₂ (purity 99.998%) and 0.0006 slm CO₂ (purity 99.998%), is passed. The CO₃⁻ reactant ions are produced by a high-frequency glow-discharge capillary-tube ion source (CIS) developed by our group (Möhler and Arnold, 1991) and meanwhile further improved in our laboratory. Hydration of the CO₃⁻ source ions occurs by association reactions with water vapor in the main flow tube. Within the 51 cm between the CIS and the mass spectrometer (IMR section, see Fig. 1) the CO₃⁻(H₂O)_n reactant ions undergo ion-molecule reactions (IMR) with the trace species SO₂ and HNO₃. The SO₂ detection scheme has been introduced by Möhler et al. (1992) and confirmed by Seeley et al. (1997):



Atmospheric measurements of gas-phase HNO₃ and SO₂

M. Hanke et al.

Title Page

Abstract

Introduction

Conclusions

References

Tables

Figures

◀

▶

◀

▶

Back

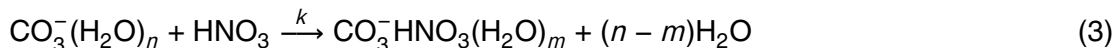
Close

Full Screen / Esc

Print Version

Interactive Discussion

The detection of gaseous HNO₃ proceeds via



(Möhler and Arnold, 1991; Schneider et al., 1998). A recent study has reinvestigated this IMR and confirmed our rate coefficients (Guimbaud et al., 1998). After having passed the IMR section, the reactant and product ions enter the mass spectrometer through a 0.15-mm diameter inlet orifice (pressure in the spectrometer $\approx 10^{-4}$ mbar, maintained by a turbo-molecular pump sustained by a mechanical pump, pumping power 2200 L/sec), where they are mass-selected and detected. The mass spectrometer is operated in the mass scan mode. One mass scan (10–200 amu) lasts 3.2 s representing the highest time resolution of the measurements. For improving the statistics, however, an integration time of 64 s (equal to 20 mass scans) has been chosen. In principle, the concentrations of SO₂ and HNO₃ ([A]) can be derived from the measured ratio *R* of product- to educt-ion count rates, the measured reaction time between the ion source and the mass spectrometer τ and the rate constants *k* of the relevant ion-molecule reactions according to $[A] = (k \times \tau)^{-1} \times \ln(1 + R)$ (e.g. Knop and Arnold, 1987). Due to experimental uncertainties, however, in situ calibrations with standards are required (see below, Sect. 2.3). Pressure, temperature, dew-point temperature, and flow are continuously monitored in the flow-tube reactor by respective sensors and recorded by using Labview. The gas flow and thus the conditions in the flow reactor are kept constant using a throttle valve at the entrance of the SCROLL pump.

2.2. Inlet for sampling ambient air

In particular with regard to measuring gas-phase HNO₃, which readily adsorbs on many materials commonly used in measurement instruments due to its sticky character (cf. Neuman et al., 1999), special care had to be paid for the design of the sampling line including the background-measurement and calibration set-up. By contrast to HNO₃ our lab studies have shown that SO₂ is not affected by adsorption on and/or desorption from sampling-line surfaces (Teflon and stainless steel). Unfortunately, in contrast to

**Atmospheric
measurements of
gas-phase HNO₃
and SO₂**M. Hanke et al.

[Title Page](#)[Abstract](#)[Introduction](#)[Conclusions](#)[References](#)[Tables](#)[Figures](#)[◀](#)[▶](#)[◀](#)[▶](#)[Back](#)[Close](#)[Full Screen / Esc](#)[Print Version](#)[Interactive Discussion](#)

inlet systems for aircraft-borne measurements of HNO₃ (Kondo et al., 1996; Ryerson et al., 1999), attention has only recently been directed to the development of a proper sampling system for ground-based and long-term continuous measurements of HNO₃ in the boundary layer where the air is usually characterized by high relative humidities and heavy aerosol loading (Huey et al., 1998; Fehsenfeld et al., 1998; Furutani et al., 2002; Mauldin et al., 1998; Neuman et al., 1999).

In principle it is desirable to keep the sampling line as short as possible to alleviate the wall effects. Yet close to the ground and/or close to other surfaces such as the walls of buildings, the concentrations of HNO₃ can be easily perturbed because of its stickiness and relatively high deposition velocity. On that score a sampling line of several meters is required for ground-based measurements to be sufficiently far above the ground and away from other surfaces. To meet these requirements we decided to set up a measuring container housing the CIMS instrument upwind from the CNR station with respect to the main wind direction (prevailing winds blow from SW) as shown in Fig. 2. The right lower corner of Fig. 2 shows a blow-up of the sampling line with the inlet approximately 5 m above the ground and about 1 m above and in front of the container and pointing in the main wind direction. Hence at least for winds from E to WSW, the air should not have encountered any surfaces before being drawn into the sampling line. According to the study of Neuman et al. (1999) the best materials for sampling HNO₃ are fluoropolymers, such as PFA, TFE, and FEP, which should be heated at least above 10°C to optimize the transmission efficiency of HNO₃. For this reason, heated Teflon for the sampling line and for the tubular inlay of the FR (see above) was chosen. The length of the PFA sampling tube with an inner diameter of 9.3 mm was 4 m. The tubing was evenly wrapped with flexible heating bands. Throughout the length of the tubing several sensors controlled the temperature. The heating was automatically regulated to keep the temperature of the tubing constant. A temperature of 40°C was chosen in order to be well above the ambient temperature variation (in general between 3°C and 19°C) and the temperature variation inside the weather-proof wrapping of the sampling line and heating bands (see Fig. 2) caused by heating due to

the direct exposure to the sunlight.

Neuman et al. (1999) have also shown that HNO_3 adsorption on PFA increases with relative humidity in the tube. This, however, might lead to some implications on Monte Cimone because of the relatively high ambient RH (mean ambient RH of 72%), strong variations in RH and the frequent exposure of the measuring site to passing and/or stationary clouds. For this reason we decided to operate the sampling line under a reduced pressure of 50 mbar, thus reducing the relative humidity to less than 2%. Another advantage of pressure reduction is that the residence time of the sampled air is reduced to 50–60 msec in contrast to 300 msec at ambient pressure. In addition earlier lab studies have shown that under ambient pressure it takes much more time to reach equilibrium between adsorption and desorption leading to a longer response time of the instrument. Heating of the sampling line and pressure reduction, however, may imply a drawback. HNO_3 contained in the aerosol, in particular in the form of solid or aqueous ammonium nitrate, may evaporate due to the equilibrium shift caused by the increase of temperature and decrease of RH in the sampling line (cf. Seinfeld and Pandis, 1997). Thus under certain atmospheric conditions, it might be rather difficult to distinguish between HNO_3 resulting from evaporation of aerosol in the sampling line and ambient atmospheric gas-phase HNO_3 (the desired parameter). This will be particularly the case in ammonia-rich air when the aerosol is neutralized or slightly alkaline, and NH_3 that did not react with sulfate will be available to react with nitrate (cf. Seinfeld and Pandis, 1997). This issue will be further discussed below.

The sampling line was regularly flushed with dry nitrogen and heated above 80°C for several hours to recondition the inner tubular surfaces.

2.3. Background measurements and calibration of CIMS

Experimental uncertainties in the CIMS method mainly comprise the difference between ion velocity and neutral velocity in the flow reactor, the rate constants of the ion-molecule reactions, the mass discrimination in the mass spectrometer, and possible wall effects in the sampling line. Therefore, in situ calibrations are the key to reli-

**Atmospheric
measurements of
gas-phase HNO_3
and SO_2**

M. Hanke et al.

Title Page

Abstract

Introduction

Conclusions

References

Tables

Figures

◀

▶

◀

▶

Back

Close

Full Screen / Esc

Print Version

Interactive Discussion

**Atmospheric
measurements of
gas-phase HNO₃
and SO₂**

M. Hanke et al.

[Title Page](#)[Abstract](#)[Introduction](#)[Conclusions](#)[References](#)[Tables](#)[Figures](#)[◀](#)[▶](#)[◀](#)[▶](#)[Back](#)[Close](#)[Full Screen / Esc](#)[Print Version](#)[Interactive Discussion](#)

able measurements of trace gases. Apart from the addition of standards, background measurements are a prerequisite for most diagnostic studies that are necessary for a thorough characterization of the instrument. Our laboratory tests have shown that dry synthetic air from gas cylinders is not suitable for background measurements, since switching ambient air to dry synthetic air alters the humidity in the flow-reactor system and thus the equilibrium between adsorption and desorption of HNO₃ on respectively from the surface. Furthermore, background measurements under ambient conditions should teach us more about potential effects resulting from variations in air composition. With respect to calibration measurements it is desirable to obtain a calibration factor under realistic ambient conditions. Hence it is required to produce a constant background signal under ambient conditions to which the standard gas can be added.

With regard to SO₂ background the sample air is passed through an activated charcoal filter (Sofnocarb, Molecular Products) by opening valves V3 and V4 and closing valves V1 and V2 (see Fig. 3) thus providing zero air free of SO₂ but with approximately ambient water vapor content. All valves are 2-way PFA valves (PARCOM).

The addition of the SO₂ standard to the sample flow is relatively straightforward. A certified gas mixture of 1.45 ppmv SO₂ in N₂ (purity 5.0) filled in a gas cylinder (Messer Griesheim, Germany) was used as SO₂ standard. For SO₂ calibration the valves in Fig. 3 were switched to the SO₂ background mode to guarantee a constant background signal and then flows of this gas mixture in the range of 0.002 to 0.03 slm (the flow was regulated by a calibrated mass-flow controller) were injected into the sample flow through “SO₂-cal-inlet” port and V6 (see Fig. 3). These flows correspond to concentrations of SO₂ in the 100 pptv – 3 ppbv range by taking into account the dilution by the higher sample flow. The delivery line (6 mm OD Teflon tubing, length = 4 m) was flushed for 2 h with this gas mixture before calibration.

A typical SO₂ calibration/measurement sequence, chosen from 6 July 2000, is presented in Fig. 4 as the time history of the measured ratio of the ion count rates ($R = [\text{SO}_5^-(\text{H}_2\text{O})_n]/[\text{CO}_3^-(\text{H}_2\text{O})_n]$, where $[\text{SO}_5^-(\text{H}_2\text{O})_n]$ constitutes the count rate of the product ions and $[\text{CO}_3^-(\text{H}_2\text{O})_n]$ the count rate of the educt ions) from which the SO₂

**Atmospheric
measurements of
gas-phase HNO₃
and SO₂**

M. Hanke et al.

Title Page

Abstract

Introduction

Conclusions

References

Tables

Figures

◀

▶

◀

▶

Back

Close

Full Screen / Esc

Print Version

Interactive Discussion

concentration is derived. The plot shows at first measurements of ambient SO₂, before, at 14:50 LT, the system was switched to SO₂ background measurements with the activated charcoal filter. Subsequently at 15:07 LT SO₂ standard gas corresponding to 1350 pptv was added, at 16:28 LT the SO₂ was increased up to 2403 pptv SO₂, and finally at 16:52 LT the standard gas was switched off and the system was in the background mode again. In this plot the linearity of the system with regard to SO₂ changes can be reproduced after subtracting the background signal. The background signal corresponds to about 130 pptv and was found to be constant throughout the campaign, i.e. independent of variations of the composition of the ambient air. Further studies in the lab suggest that this constant background signal at mass peak 112 amu, which is also the mass of SO₅⁻, is produced in the gas-discharge ion source. The fast time response of the system when SO₂ is added and turned off again and the constant calibration factor rather exclude that this signal results from desorption from the walls. Apart from this no significant typical wall effects could be observed such as slow increase of SO₂ due to adsorption when SO₂ is added or slow decrease of SO₂ when SO₂ was turned off due to desorption from walls, or a significant change in the signal when the temperature in the flow reactor and thus of the wall surfaces was increased or decreased.

For scrubbing HNO₃ from ambient air we used a nylon filter, which has long been used as a medium to collect HNO₃ in filter measurements or as HNO₃ scrubber (Goldan et al., 1983; Huey et al., 1998) and has also shown in this study to effectively remove HNO₃ from the sample flow. For background measurements the sample air was branched off into an extra tubing with two vacuum-proof filter holders, the first containing a Teflon prefilter to remove particulate matter from the sampled air (Zefluor, pore size 1 μm, diameter 90 mm, Pall Gelman Corp.) and the second one containing a nylon filter (Nylasorb TM membrane disc filter, pore size 1 μm, diameter 90 mm, Pall Gelman Corp.). For this measurement mode valves V2 and V3 were closed (see Fig. 3) and V1 and V4 were open. The filters were replaced at least every day by clean ones.

The HNO₃ calibration source is a permeation tube (KINTEC, Type HRT, 10 cm long,

**Atmospheric
measurements of
gas-phase HNO₃
and SO₂**

M. Hanke et al.

[Title Page](#)[Abstract](#)[Introduction](#)[Conclusions](#)[References](#)[Tables](#)[Figures](#)[⏪](#)[⏩](#)[◀](#)[▶](#)[Back](#)[Close](#)[Full Screen / Esc](#)[Print Version](#)[Interactive Discussion](#)

emission rate specified by manufacturer: 1251 ng/min) stored in a 40°C temperature-controlled glass reservoir embedded in an aluminium oven (KINTEC). A constant flow of dry N₂ as carrier gas (0.19 slm controlled by a calibrated mass-flow controller) was continuously passed through the reservoir over the permeation tube to prevent accumulation of nitric acid vapor in the reservoir. During calibration the effluent of the reservoir was diluted by an N₂ dilution flow (0–7 slm regulated by a mass-flow controller) right after the reservoir exit. In this way different concentrations of HNO₃ could be produced. The HNO₃ standard gas was delivered through a PFA tubing (4 m long, 6 mm OD) to a 2-way PFA T fitting where a small portion of the flow (of the order of 0.2 slm depending on the pressure in the delivery line) was branched off and drawn through a critical orifice with a radius of 150 μm at “HNO₃-cal-inlet” port and V5 (see Fig. 3) into the low-pressure region of the sampling line. Before calibration the system was switched to HNO₃ background mode in order to have a stable background signal. The Teflon delivery line was continuously conditioned with the output of the permeation source. When the flow in the delivery line was changed, a time of several hours was given for reconditioning the wall surfaces before the HNO₃ standard gas was introduced into the sampling line. For calibrating the permeation-source output, the delivery line was detached just in front of valve V5 and attached to a sequence of two glass-washing bottles each containing 50–75 mL of deionized water. In general the effluent of the permeation source bubbled through the gas-washing system for 6 to 7 h to ensure adequate accumulation of nitrate for accurate analysis of the solution by ion chromatography. The latter was performed at our lab in Heidelberg. To check whether the emission rate of the permeation source is stable, this procedure was repeated at least every second day. An emission rate of 850–900 ng/min was determined for the period of the MINATROC campaign. The deviation from the emission rate given by the manufacturer can be explained by the aging of the permeation tube, which could be also observed by a steady decrease of the emission rate under comparable experimental conditions over the course of the year 2000.

During this campaign, calibrations were made quite frequently, in particular to mon-

**Atmospheric
measurements of
gas-phase HNO₃
and SO₂**M. Hanke et al.

[Title Page](#)[Abstract](#)[Introduction](#)[Conclusions](#)[References](#)[Tables](#)[Figures](#)[⏪](#)[⏩](#)[◀](#)[▶](#)[Back](#)[Close](#)[Full Screen / Esc](#)[Print Version](#)[Interactive Discussion](#)

itor a possible change in the sensitivity of the apparatus. Also a number of different diagnostic tests and studies such as linearity checks or variations of humidity in the sampling line were performed for a better characterization of the set-up both on site and at the MPI-K. Figure 5 shows a plot of the measured [HNO₃] (derived similarly to formula (4) in Schneider et al., 1998, and taking into consideration effects like pressure dilution, flow dilution, etc.) versus time during a typical HNO₃ background-calibration-background sequence carried out on 26 June 2000 on Monte Cimone. At 13:40 LT the valves V1, V2, and V4 were switched to pass the ambient air through the filters to remove ambient HNO₃ as described above. In general within a period of 4 min, the signal dropped down to 1/e of the HNO₃ level present just before the instrument was switched into the background mode (BG). After about 20–30 min the background signal reached its near steady-state level. This background seems to be composed of two components. The first component seems to be mainly due to desorption of HNO₃ from the walls of the flow tube. The second component of the HNO₃ BG was found to be rather constant at levels around 30–40 pptv. The total background was found to show a slight dependence on the ambient water-vapor content according to $[\text{HNO}_3]_{\text{BG}} = (34.7 + 0.0054 \times [\text{H}_2\text{O}]_{\text{ambient}})$ pptv with $[\text{H}_2\text{O}]_{\text{ambient}}$ given in units of ppmv. A clear scaling of the BG with ambient HNO₃ could not be seen. The water-vapor dependence indicates that the interaction between surface and sampled air is enhanced with increasing water vapor in the air. These findings would be in accordance with the observations of Neuman et al. (1999), who, as already mentioned above, found that the adsorption of HNO₃ on PFA increases with relative humidity in the tube, i.e. in the background mode more HNO₃ should desorb from the walls if the process of adsorption is reversible. Waiting long enough, i.e. longer than 2 h, allowed the background to reach a constant value a little bit above the electronic noise level. This constant contribution to the BG could result from impurities contained in the source gas of the ion source. For our data analysis we considered the near steady-state background after 20 min to be appropriate since it accounts best for the response time with regard to HNO₃ due to the equilibrium between desorption and adsorption on the walls. The so

determined background level of HNO_3 , which had to be subtracted from the measured signal, varied between 45 pptv and 115 pptv under the prevailing conditions on Monte Cimone.

In Fig. 5, at 14:24 LT HNO_3 standard gas corresponding to 1036 pptv was added. After about 10 min the system reached the equilibrium level. Linearity checks, i.e. increasing or decreasing the concentration of the added HNO_3 (400 pptv – 4500 pptv) during a calibration sequence, have shown that usually the instrument reaches the equilibrium level within a shorter period of time, i.e. within 4 to 5 min. The longer response time as shown in Fig. 5 is probably caused by the conditioning of the final 15 cm of the 6 mm-OD Teflon tubing through which a flow of about 0.2 slm is branched off from the delivery line into the sampling line as described above. This short part of tubing cannot be conditioned before calibration. During a linearity check a longer response time is only seen when HNO_3 is first added. When the HNO_3 concentration is subsequently altered, a shorter response time is observed. At 15:11 LT the calibration gas was turned off and the instrument was in the background mode again. At 15:46 LT the valves V1, V2, and V4 were switched back to measure ambient HNO_3 again. Our calibration and diagnostic measurements have confirmed the results of Neuman et al. (1999), that Teflon tubing maintained above 10°C guarantees a low adsorption of HNO_3 (<20%) and that the adsorption increases in humid sampling environments. The latter effect, however, did only affect the value of our background signal, but did not exert a significant influence on our calibration factor.

Concerning both SO_2 and HNO_3 additional tests were carried out to characterize the parts of the sampling line that were not taken into account by the background and calibration measurements described above. These parts include the inlet orifice, the part of the sampling line before valves V1 and V2 (about 1 m) and the part of the sampling line between V2 and the T fitting close to V4 (about 34 cm) (see Fig. 3) and the valves themselves. These tests comprised the addition of zero air in front of the inlet orifice to check for possible memory effects not considered by the above-described diagnostic measurements and the addition of calibration gas right after the inlet orifice.

**Atmospheric
measurements of
gas-phase HNO_3
and SO_2** M. Hanke et al.

[Title Page](#)[Abstract](#)[Introduction](#)[Conclusions](#)[References](#)[Tables](#)[Figures](#)[⏪](#)[⏩](#)[◀](#)[▶](#)[Back](#)[Close](#)[Full Screen / Esc](#)[Print Version](#)[Interactive Discussion](#)

**Atmospheric
measurements of
gas-phase HNO₃
and SO₂**M. Hanke et al.

[Title Page](#)[Abstract](#)[Introduction](#)[Conclusions](#)[References](#)[Tables](#)[Figures](#)[◀](#)[▶](#)[◀](#)[▶](#)[Back](#)[Close](#)[Full Screen / Esc](#)[Print Version](#)[Interactive Discussion](#)

The two different background signals agree very well under comparable atmospheric conditions. No perceivable effects could be observed. Hence, these studies showed that under the operational conditions of our PFA sampling line (50 mbar, 40°C, about 12.4 slm flow) the above-described background measurements are representative for the entire sampling line, even if about 1.3 m were not considered. In addition, other studies with 1/2 inch heated PFA sampling lines of different lengths (4 m and 1 m) yielded similar results. If the calibration gases are added right after the inlet orifice and compared to the calibration measurements as described above, also no perceivable difference between the calibration factors could be observed for different atmospheric conditions. Furthermore, before and after the campaign the inlet orifice was checked for possible memory effects and characterized, too.

The detection limit (2σ) for HNO₃ that is dependent on the background level was 30–50 pptv. For SO₂ the detection limit was 30–40 pptv. The precision for both trace gases was 4%. The accuracy for HNO₃ is a function of the background and varied between 20% and 45%. For SO₂ the accuracy is about 20–30%.

3. Results and discussion

3.1. Data overview

In the intensive measurement period between 1 June and 6 July 2000 almost continuous 24-hour measurements of HNO₃ and SO₂ were made with CIMS with the exceptions of the periods 1–3 June, when the instrument was checked and tuned, 11–13 June, when the instrument had to be turned off because of severe weather conditions such as rain and thunderstorms, and 20–22 June because of a pump failure. On 24 June diagnostic measurements were carried out with respect to HNO₃. Figure 6 shows the time series (30-min average data) of HNO₃ (uppermost panel) and SO₂ (second panel). Frequently in the late afternoons or in the early evenings, the instrument had to be turned off because of thunderstorms or rain, or because of diagnostic measure-

**Atmospheric
measurements of
gas-phase HNO₃
and SO₂**

M. Hanke et al.

[Title Page](#)[Abstract](#)[Introduction](#)[Conclusions](#)[References](#)[Tables](#)[Figures](#)[⏪](#)[⏩](#)[◀](#)[▶](#)[Back](#)[Close](#)[Full Screen / Esc](#)[Print Version](#)[Interactive Discussion](#)

ments, which were preferably performed at this time of the day. The high HNO₃ values of 28 June afternoon should be considered rather carefully because at about 14:00 LT the site became wrapped in clouds and condensation occurred on the sampling orifice due to malfunction of the orifice heating. Therefore it is likely that cloud water that condensed and thus was accumulated on the outer surface of the sampling orifice was drawn into the sampling system where it could have evaporated and released HNO₃.

Along with the CIMS instrument we also operated a commercial UV absorption instrument (Thermo Environmental Instruments 49 C, detection limit 1 ppbv with a total uncertainty of 1 ppbv, 1 min time resolution) to measure the concentration of O₃ at our container. The third panel of Fig. 6 shows the time series of O₃ obtained between 3 June and 6 July 2000. An additional measurement of O₃ was performed at the station by CNR-ISAO (UV-Absorption Dasibi, inlet about 8 m above the ground at the CNR-ISAO observatory station; see Bonasoni et al., this issue). A correlation plot yields O₃ (CNR-ISAO) = 4.9 + 0.9 × O₃ (MPI-K), r² = 0.82. According to this the CNR-ISAO instrument tends to measure lower values than the MPI-K instrument does.

Below the O₃ panel in Fig. 6 the local wind direction measured by CNR-ISAO (Bonasoni et al., this issue) is presented. The lowermost panel of Fig. 6 classifies the air masses according to their origin from the Arctic, North Western, Western, or Eastern Europe, the Mediterranean basin, Saharan Africa without dust and containing dust. This classification is deduced from 144-h three-dimensional back trajectories calculated every three hours with the FLEXTRA trajectory model (Stohl et al., 1995). The geographical regions over which the air masses spent most of their time before reaching Monte Cimone define the classes. A further subdivision, shown in the fifth panel (marked as altitude classification) of Fig. 6, in ascending air masses from the boundary layer and descending air masses from the free troposphere has been made depending on the vertical displacement of the back trajectories (Balkanski et al., this issue; Putaud et al., this issue; van Dingenen et al., this issue). Table 1 shows the mean levels of the HNO₃, SO₂, and O₃ concentrations (mean ± 1 σ deviation) for the different air masses. The second column of this table gives the subdivision in ascending air masses from

**Atmospheric
measurements of
gas-phase HNO₃
and SO₂**

M. Hanke et al.

[Title Page](#)[Abstract](#)[Introduction](#)[Conclusions](#)[References](#)[Tables](#)[Figures](#)[⏪](#)[⏩](#)[◀](#)[▶](#)[Back](#)[Close](#)[Full Screen / Esc](#)[Print Version](#)[Interactive Discussion](#)

the boundary layer and descending air masses from the free troposphere. Similar to the measurements of Fischer et al., this issue, the differences in the trace-gas levels for different air-mass classes are relatively small. In general air masses descending from the free troposphere show lower levels of pollution, in particular air masses from the Arctic region. One major exception is the mean level of SO₂ of Mediterranean origin. In contrast to the boundary-layer value the value for the free troposphere is twice as high. This value is also marked with a relatively high standard deviation, which is due to an SO₂ event of approximately 2 h that occurred in the morning between 06:00 and 08:00 LT on 9 June. Without this event the mean SO₂ value for the FT would be (0.387 ± 0.333) ppbv. The increase of SO₂ up to above 8 ppbv at this day coincides with a change of wind direction (from ~200° Tuscany) to ~300° (Po area which is more polluted), a dip in O₃, a rapid drop of the relative humidity from 90% down to 45%, and a peak of sulfate contained in aerosol (Putaud et al., this issue; van Dingenen et al., this issue). With regard to HNO₃ highest levels of ~1.2 ppbv are observed for air masses ascending from the boundary layer and spending most of their time over NW Europe. With regard to SO₂ highest levels are observed for air masses staying most of their time in the boundary layer either over E Europe, a region of high emissions of sulfur compounds, or Africa. Most of the latter back trajectories somehow passed over the region of Lazio and Tuscany, possible emission sources of SO₂, before reaching Monte Cimone. Another evident feature in Table 1 is that, for air masses ascending from the boundary layer and spending most of their time in the African area, the mean level of HNO₃ for air masses with dust is only half of the mean level without dust. SO₂ and O₃ also show smaller values for the air masses containing dust, but the differences are not as striking as for HNO₃. Looking at the back trajectories of the single days and comparing the ones from Africa with and without dust, one can see that most of the back trajectories of the African air masses without dust passed over Lazio and Tuscany before they reached Monte Cimone, while the air masses from Africa with dust took the route directly from the Mediterranean Sea via Corsica. This might be taken into account for the interpretation of these data. Nevertheless, ignoring the possibility that these air

**Atmospheric
measurements of
gas-phase HNO₃
and SO₂**

M. Hanke et al.

[Title Page](#)[Abstract](#)[Introduction](#)[Conclusions](#)[References](#)[Tables](#)[Figures](#)[◀](#)[▶](#)[◀](#)[▶](#)[Back](#)[Close](#)[Full Screen / Esc](#)[Print Version](#)[Interactive Discussion](#)

masses might have had different chemical histories, one might conclude that the direct impact of dust is stronger on HNO₃ than on SO₂ and O₃ (see also discussion).

Not considering the data during a major dust intrusion between 3 and 4 July, lowest levels of HNO₃ and SO₂ with a mean level of 360 ± 150 pptv for HNO₃ and 150 ± 180 pptv for SO₂ were observed during the nights of 5/6 June, 19/20 June and 22/23 June. This parallels the observations of NO_x, NO_y, CO, and HCHO (Fischer et al., this issue) and the low concentrations of condensation nuclei (CNC) (Putaud et al., this issue; van Dingenen et al., this issue). Furthermore a drop of the relative humidity below 40% and an enhancement of CO₂ (Bonasoni et al., this issue) during these periods indicate downward transport of air from the free troposphere (Fischer et al., this issue).

Table 2 presents statistical summaries of all, daytime, and nighttime mixing ratios of HNO₃, SO₂, and O₃ measured at the site between 3 June and 5 July 2000. Daytime is defined as 08:00–22:00 LT (= 06:00–20:00 GMT) and nighttime as 22:00–08:00 LT. With regard to HNO₃ it is distinguished between the data containing the rather uncertain cloud data of 28 June and those without these data. All mixing ratios reported in this table are based on 30-min averages integrated over the measurement period. In accordance with the NO_x, NO_y, CO, and HCHO data of Fischer et al. (this issue), relatively low daytime median levels of HNO₃ (777 pptv), SO₂ (254 pptv), and O₃ (59 ppbv) are observed. This suggests that in general this site was not heavily affected by local pollution during the period of the campaign except for some pollution events of short duration such as the one on 9 June (see Fig. 6). During the night the median levels for HNO₃ and SO₂ are slightly lower with 704 pptv and 228 pptv, respectively, while the level for O₃ (63 ppbv) is slightly higher. For the period between 3 June and 30 June of combined measurements with MPI-CH we obtain a ratio NO_x/HNO₃ ~ 0.3 (NO_x taken from Fischer et al., this issue) with regard to daytime median levels. This agrees with the conclusion of Fischer et al. (this issue) that rather photochemically aged air masses were probed at this site.

The diurnal variations of HNO₃, SO₂ and O₃ during the measuring period are relatively weak as can be seen in Fig. 7. With regard to HNO₃ the uncertain data of 28

**Atmospheric
measurements of
gas-phase HNO₃
and SO₂**

M. Hanke et al.

[Title Page](#)[Abstract](#)[Introduction](#)[Conclusions](#)[References](#)[Tables](#)[Figures](#)[⏪](#)[⏩](#)[◀](#)[▶](#)[Back](#)[Close](#)[Full Screen / Esc](#)[Print Version](#)[Interactive Discussion](#)

June are ignored. A slight enhancement with a relatively large deviation can be observed for SO₂ in the morning period between 06:45 and 08:15 LT, which is due to a bias in the morning data of 9 June. Diurnal variations due to the local meteorology of a high-elevation mountainous site, as explained in Fischer et al. (this issue), and might be expected at Monte Cimone, are not really obvious, as it is also the case for NO_x, NO_y, and CO measured by Fischer et al. (this issue).

3.2. Comparison of HNO₃ with NO_y

As already mentioned above, also NO_y measurements were carried out by the Max-Planck-Institute for Chemistry (Fischer et al., this issue) at the nearby CNR-ISAO laboratory building. NO_y was sampled at a height of 8 m above the roof of the CNR building using a telescope mast. The distance between the HNO₃ sampling inlet of the CIMS instrument and the inlet of the NO_y instrument was about 50–60 m.

The calculated mean value of the ratio between HNO₃ and NO_y is 0.9 with a standard deviation of 2.8. 39% of all ratios are higher than one. Figure 8 shows a correlation plot of HNO₃ versus NO_y, based on the 30-min average data. The linear regression renders (HNO₃ = 0.36 NO_y + 0.48) ppbv with a correlation of $r^2 = 0.2$ for 505 data points, i.e. the correlation can be called significant. The correlation is even better if the uncertain HNO₃ data points of 28 June are ignored ($r^2 = 0.3$ for 498 data points). However, the significant offset of almost 0.5 ppbv yielded by the linear regression causes some concern. This offset can be either due to an overestimation of HNO₃ or a corresponding underestimation of the NO_y values. With respect to the NO_y measurements this point has been addressed by Fischer et al. (this issue). With regard to the CIMS instrument a constant instrumental offset of ~ 0.5 ppbv can be excluded as shown by our diagnostic measurements such as background measurements and the linearity checks (multipoint calibration checks) carried out both at site and before and after the campaign in the laboratory. Furthermore, the atmospheric measurements of HNO₃ frequently yielded values down to 30–50 pptv (which is the level of the in-

strumental detection limit), also being an indication that an instrumental offset is not present for the CIMS system.

Another possible source for gaseous HNO_3 could be the decomposition and evaporation of NH_4NO_3 particles in the sampling line due to the heating and the pressure reduction of the carrier gas as already discussed above in the “Experimental Section”. Therefore, calculations with the aerosol behavior code NACHE (Bunz and Dlugi, 1991) were performed on the basis of best-guess data for the size distribution and composition of the aerosol particles to estimate the contribution of evaporating aerosol particles to the concentration of gaseous HNO_3 . The modules to simulate the condensation and evaporation of NH_4NO_3 particles were verified and implemented into the code during extensive experimental and theoretical investigations of the distribution of NH_4NO_3 within an ensemble of mixed aerosol particles (Bunz et al., 1995; Saathoff et al., 1995). According to this estimate for a residence time of approximately 160 msec in the sampling line, a pressure of 50 mbar and a temperature of approximately 40°C inside the flow-tube system, less than 1% of the volatile volume of the coarse-mode aerosol with a mass median diameter of $1.5\ \mu\text{m}$ and a standard deviation of 2 (see Putaud et al., this issue; van Dingenen et al., this issue) should be susceptible to evaporation. The meteorological data measured during the campaign at Monte Cimone (see Bonasoni et al., this issue) show that the relative humidity was above 70–80% under nearly all conditions so that the deliquescence point of NH_4NO_3 was exceeded and the aerosol was probably wet at the inlet of the CIMS. But the evaporating aerosol fraction mentioned above was calculated assuming that the particles are dry at the inlet. Therefore, the value of 1% can be regarded as an upper limit since on the one hand the process to dry the particles is quite slow and very likely incomplete after 160 msec (ten Brink and Veefkind, 1995) and on the other hand wet particles evaporate much slower than dry particles due to the lower vapor pressure of NH_3 and HNO_3 over solutions in comparison to the solid phase. The evaporation of the smaller particles (fine mode) (see Putaud et al., this issue; van Dingenen et al., this issue) most probably would proceed faster. In order to assess a maximum of possible interference from aerosol evapora-

**Atmospheric
measurements of
gas-phase HNO_3
and SO_2** M. Hanke et al.

Title Page

Abstract

Introduction

Conclusions

References

Tables

Figures

◀

▶

◀

▶

Back

Close

Full Screen / Esc

Print Version

Interactive Discussion

**Atmospheric
measurements of
gas-phase HNO₃
and SO₂**

M. Hanke et al.

[Title Page](#)[Abstract](#)[Introduction](#)[Conclusions](#)[References](#)[Tables](#)[Figures](#)[⏪](#)[⏩](#)[◀](#)[▶](#)[Back](#)[Close](#)[Full Screen / Esc](#)[Print Version](#)[Interactive Discussion](#)

tion, it has been assumed that the total volume of the coarse mode (see Putaud et al., this issue; van Dingenen et al., this issue) was made of liquid HNO₃ and 1% of it would evaporate into the gas phase. In addition it was assumed that the contribution of the fine mode to the aerosol would evaporate. For this the nitrate concentration of the submicron aerosol measured on-line using a steam-jet aerosol collector combined with a wet annular denuder by JRC, Ispra, on Monte Cimone (Putaud et al., this issue; van Dingenen et al., this issue) was converted into gas-phase mixing ratio and added to the possible contribution of the coarse mode. The estimated aerosol contribution is then subtracted from the measured HNO₃. The result is shown in Fig. 9. According to this estimate an 18% contribution from the aerosol phase to the measured gas-phase HNO₃ signal would result as median deviation from the measured HNO₃ with the central 50% ranging between 7% and 40%. Inspecting the correlation with NO_y we would obtain the relation HNO₃ – estimated aerosol contribution = 0.91 – 0.0003 × NO_y with a correlation coefficient of $r^2 = 0.08$ when the negative values are included and 0.46 + 0.0002 × NO_y with $r^2 = 0.08$ when the negative values are ignored. For sure these correlations do not represent anything realistic. This is already evident from Fig. 9 showing that on some days the potential interference from the aerosol phase is by far overestimated leading to extreme negative values. Figure 9 also shows that the problem with the offset of 0.5 ppbv cannot be explained by a possible HNO₃ contribution to the gas-phase signal resulting from the evaporation of aerosol. In particular on those days when HNO₃ is higher or at the same level as NO_y no significant contribution to the gas-phase measurements of HNO₃ from the aerosol phase can be expected. This study demonstrates very well that the degree of uncertainty related to the interference from aerosol evaporation in the sampling line assessed above represents an upper limit and does not increase the uncertainty of the HNO₃ measurements beyond the uncertainty limits of the instrument given above. The only conditions that might increase the uncertainty of the CIMS technique are conditions of clouds and rain, i.e. when water could condense/accumulate on the outside surface of the sampling line and finally was drawn into the sampling line because it could not be evaporated fast enough by the

**Atmospheric
measurements of
gas-phase HNO₃
and SO₂**M. Hanke et al.

[Title Page](#)[Abstract](#)[Introduction](#)[Conclusions](#)[References](#)[Tables](#)[Figures](#)[⏪](#)[⏩](#)[◀](#)[▶](#)[Back](#)[Close](#)[Full Screen / Esc](#)[Print Version](#)[Interactive Discussion](#)

outside orifice heating, either because of malfunction of the heating or because of too much water. However, by scrutinizing our housekeeping data all that data was carefully sorted out apart from the data obtained on 28 June. On that day it was not that evident from the housekeeping. Only some remarks in the data protocol pointed out some problems with the heating. Hence we decided to show this data, although it is marked with a question mark. Based on our measurements, both diagnostic and atmospheric, and on this estimate we consider a systematic overestimation of 0.5 ppbv by CIMS as very unlikely. It seems that the discrepancy between the HNO₃ and NO_y measurements of Monte Cimone cannot be solved that easily and needs further investigation. However, it is rather difficult to find the answer after the experiment is over. Therefore, it would be desirable to carry out HNO₃ spike tests with both instruments under different meteorological conditions at the next MINATROC campaign, as have been already performed with CIMS on Monte Cimone. For the next campaign (MINATROC 2002), in order to reduce the uncertainty related to a possible evaporation of aerosol in our sampling line, we redesigned our sampling system in such a way that the residence time could be decreased down to about 100 msec. This has been achieved by a blower inlet pipe with an inner diameter ID of 60 cm through which the ambient air is drawn in with a velocity of 10–15 m/s. After approximately 100 msec the air is sampled from the center of the pipe vertically to the flow. In this way the degree of collecting aerosol is also reduced. Furthermore, this new inlet also allows to measure under conditions of dense fog/clouds and precipitation. We tested the new inlet system carefully during a campaign (SCAVEX) on the Environmental Research Station “Schneefernerhaus” located on Zugspitze, Germany, and the results were very promising. In these tests we also compared the relatively long sampling system of Monte Cimone with the new system and could not find any significant difference. This campaign also allowed us to compare our instrument with another technique to measure HNO₃ operated by DLR, Oberpfaffenhofen, and so far, based on the preliminary data analysis, we found good agreement between these two different techniques.

3.3. Mineral dust event of 3–4 July

During the period of 3 and 4 July 2000 an intensive episode of dust transport over the Mediterranean Sea and over the MTC site was recorded. (Bonasoni et al., this issue; Balkanski et al., this issue; Gobbi et al., this issue; Putaud et al., this issue; van Dingenen et al., this issue).

During this period a large cloud of dust was detected over the Mediterranean Sea and at the site as shown by satellite, sun photometers, optical counters and ion chromatography (Balkanski et al., this issue; Putaud et al., this issue; van Dingenen et al., this issue). Air-mass back trajectories showed direct transport of air masses originating at ground level over Morocco and Algeria, over the Mediterranean, towards the site. By 11:00 LT of 3 July the bottom of the dust cloud had descended down to approximately 2000 m asl (i.e. to include the Mt. Cimone station), while its top reached up to 8 km altitude. Dust and clouds were still present up to 6 km on 4 July at 12:00 UTC (Gobbi et al., this issue). At around 04:00 LT on 4 July the dust monitor on MTC measured the highest concentrations of particles (a maximum of 3.2 particles/cm³ (size > 1 μm, JRC Ispra + CNR-ISAO) (Putaud et al., this issue; van Dingenen et al., this issue).

Figure 10 shows the measured concentrations of HNO₃, SO₂ and O₃ during the dust event together with the average bi-diurnal trends. At the onset of the dust event the HNO₃ concentration started to decrease continuously and reached its minimum in the early morning of 4 July. After a short period of passing clouds and slight rain at around noon of 4 July HNO₃ recovered again. The efficient removal of HNO₃ from the gas phase by mineral dust would be in agreement with laboratory studies of Hanisch and Crowley (2001a, 2002) showing that the uptake of HNO₃ by dust surfaces is very efficient. In contrast to HNO₃ the SO₂ mixing ratio does not show such a clear influence of dust. A decrease of the O₃ concentration is demonstrated compared to the non-dust episode.

To show the possible effect of mineral dust on HNO₃, SO₂ and O₃ the concentrations of these gases are plotted versus the integrated surface area concentration for parti-

**Atmospheric
measurements of
gas-phase HNO₃
and SO₂**

M. Hanke et al.

Title Page

Abstract

Introduction

Conclusions

References

Tables

Figures

⏪

⏩

◀

▶

Back

Close

Full Screen / Esc

Print Version

Interactive Discussion

**Atmospheric
measurements of
gas-phase HNO₃
and SO₂**

M. Hanke et al.

[Title Page](#)[Abstract](#)[Introduction](#)[Conclusions](#)[References](#)[Tables](#)[Figures](#)[◀](#)[▶](#)[◀](#)[▶](#)[Back](#)[Close](#)[Full Screen / Esc](#)[Print Version](#)[Interactive Discussion](#)

cles with size > 721 nm (S) measured with DMA/OPC (see Putaud et al., this issue; van Dingenen et al., this issue) in Fig. 11. It is also distinguished between increasing surface area of the coarse particles (between 08:45 LT 3 July and 03:45 LT 4 July) and decreasing surface area after the peak surface area concentration has been reached at around 04:00 LT (between 04:45 4 LT July and 18:45 LT 4 July). All three trace gases show a clear negative correlation with S. The linear regression yields are shown in Table 3. Both HNO₃ and O₃ show highly significant correlations whereas the significance for the correlation between SO₂ and S is less pronounced.

Looking at the integrated surface area of the particles < 559 nm positive correlations are found between the surface area and the concentrations of HNO₃, SO₂ and O₃ as shown in Fig. 12. This might be an indication of the mixing of relatively fresh polluted boundary-layer air with the air coming from Africa and containing the dust. The results of the linear regressions are shown in Table 4.

Unfortunately a full chemical characterization of the air mass during this dust event is not possible due to the lack of NO, NO₂, NO_y, CO, and HCHO, which were not measured anymore after 30 June and which would have allowed an insight into transport processes and hence the mixing of polluted air masses with the dust cloud.

4. Summary

For the first MINATROC field campaign on Monte Cimone in Italy MPI-K Heidelberg developed and built an improved CIMS instrument for continuous ground-based measurements of gas-phase HNO₃ and SO₂ under atmospheric conditions with relatively high humidities typically encountered in the boundary layer or lower free troposphere. The principle of the instrument relies on ion-molecule reactions with CO₃⁻ ions, which are produced with a capillary-tube gas-discharge ion source. To meet the best conditions for sampling gas-phase HNO₃ which readily adsorbs on many materials due to its sticky character, we utilized a heated PFA sampling line which was operated at a temperature of 40°C and a pressure of 50 mbar. Special attention was turned to the

**Atmospheric
measurements of
gas-phase HNO₃
and SO₂**

M. Hanke et al.

[Title Page](#)[Abstract](#)[Introduction](#)[Conclusions](#)[References](#)[Tables](#)[Figures](#)[◀](#)[▶](#)[◀](#)[▶](#)[Back](#)[Close](#)[Full Screen / Esc](#)[Print Version](#)[Interactive Discussion](#)

determination of a proper background under realistic ambient conditions for both HNO₃ and SO₂. This has been achieved by means of the combination of a Teflon and a Nylon filter for HNO₃ and an activated charcoal filter for SO₂. For calibrating the system with regard to HNO₃ the output of a HNO₃ permeation source was added to ambient air from which HNO₃ had been scavenged before by the filters. SO₂ standard was taken from a certified gas mixture. In this way for both HNO₃ and SO₂ calibration factors under realistic ambient conditions could be determined.

For the atmospheric conditions during the field campaign on Monte Cimone the detection limit (2σ) for HNO₃ showed a dependence on the background and was in the range between 20 and 50 pptv. The detection limit of SO₂ did not show such a dependence and was 30–40 pptv. The precision for both trace gases was 4%. The accuracy for HNO₃ turned out to be a function of the background level and varied between 20% and 45%. For SO₂ the accuracy was 20–30%.

Between 3 June and 6 July almost continuous 24-hour measurements of HNO₃ and SO₂ were carried out. Along with the CIMS instrument a commercial UV absorption instrument was operated to measure O₃. During this campaign relatively low mean mixing ratios of 0.78 ppbv for HNO₃, 0.37 ppbv for SO₂ and 61 ppbv for O₃ were observed. Only sporadic and relatively small contributions from local pollution could be seen. Highest levels of SO₂ and HNO₃ reached ~8 ppbv and ~2.7 ppbv (excluding the uncertain data of 28 June), respectively.

From the comparison of HNO₃ with NO_y measured simultaneously at the site by MPI-CH, the resulting regression of the correlation renders HNO₃ = (0.48 + 0.36 × NO_y) ppbv, i.e. showing a significant offset of almost 0.5 ppbv, which has to be either due to an overestimation of HNO₃ or an underestimation of NO_y. Both experimental studies and theoretical estimations of the order of magnitude of the possible interference due to evaporation of NH₄NO₃ particles releasing HNO₃ into the gas phase showed that an overestimation of HNO₃ is rather unlikely. This discrepancy between the HNO₃ measurements and the NO_y measurements cannot be solved anymore that easily after the experiment is over and therefore it is recommended to look more closely and system-

atically at this problem at another campaign in the near future.

An extension of the intensive measuring period from 30 June to 6 July gave us the chance to obtain complete data sets of HNO₃, SO₂ and O₃ before, during, and after an intrusion of mineral dust on Monte Cimone during the period of 3 and 4 July. After the onset of the dust event on 3 July the mixing ratio of HNO₃ started to decrease continuously and in the early morning of 4 July gaseous HNO₃ was virtually absent. In contrast to nitric acid the profile of SO₂ did not show any clear influence of dust. A decrease of O₃ to below 50 ppbv was also observed. Although a further characterization of the air masses is not possible because of the lack of additional important gas-phase parameters, these measurements might provide for the first time a strong observational indication of efficient uptake of gaseous HNO₃ by mineral-dust aerosol particles, which might imply as suggested, that mineral dust represents a significant sink for HNO₃ in the troposphere, and hence could have an impact on the photochemical cycles and O₃ production.

Acknowledgements. This study is part of the EU-funded project MINATROC (EVK2-CT-1999-00003) under the 5th Framework Program. We like to thank the MINATROC community and the technical staff of MPI-K, particularly Ute Schwan, the MTC team P. Bonasoni, F. Calzolari and the Magera and Giambi team. Special thanks to Dr. G. Hönes for her support and comments.

References

- Adams, J. W., Cox, R. A., Griffiths, P., and Stewart, D. J.: Reactive uptake of acidic gases on mineral aerosols, in Proceedings of the 27th General assembly of the European Geophysical Society, 21–26 April 2002, Nice, France, Geophysical Research Abstract, Vol. 4, 2002.
- Arnold, F. and Hauck, G.: Lower stratospheric trace gas detection using aircraft-borne active chemical ionisation mass spectrometry, Nature 315, 307–309, 1985.
- Arnold, F., Schneider, J., Gollinger, K., Schlager, H., Schulte, P., Hagen, D., Whitefield, P. D., and von Velthoven, P.: Observation of upper tropospheric sulfur dioxide and acetone pollution: Potential implications for hydroxyl radical and aerosol formation, Geophys. Res. Lett., 24, 57–60, 1997.

**Atmospheric
measurements of
gas-phase HNO₃
and SO₂**

M. Hanke et al.

Title Page

Abstract

Introduction

Conclusions

References

Tables

Figures

◀

▶

◀

▶

Back

Close

Full Screen / Esc

Print Version

Interactive Discussion

**Atmospheric
measurements of
gas-phase HNO₃
and SO₂**

M. Hanke et al.

[Title Page](#)[Abstract](#)[Introduction](#)[Conclusions](#)[References](#)[Tables](#)[Figures](#)[◀](#)[▶](#)[◀](#)[▶](#)[Back](#)[Close](#)[Full Screen / Esc](#)[Print Version](#)[Interactive Discussion](#)

Balkanski, Y., Bauer, S. E., Bonasoni, P., Fischer, H., Gobbi, G. P., Hanke, M., Hauglustaine, D., Putaud, J. P., Schulz, M., and Van Dingenen, R.: Overall presentation of the campaign of Mt Cimone, Italy (free troposphere); principal characteristics of the gaseous and aerosol composition from European pollution, Mediterranean influences and during African dust events, Atmos. Chem. Phys. Discuss., this issue, 2002.

Berresheim, H. and Jaeschke, W.: The contribution of volcanoes to the global sulfur budget, J. Geophys. Res., 88, 3732–3740, 1983.

Berresheim, H., Wine, P. H., and Davis, D. D.: Sulfur in the atmosphere, in: Composition, Chemistry, and Climate of the Atmosphere; (Ed) Singh, H. B., 251–307, Van Nostrand Reinhold, New York, 1995

Bonasoni, P., Stohl, A., Cristofanelli, P., Calzolari, F., Colombo, T., and Evangelisti, F.: Background ozone variations at Mt. Cimone station, Atmos. Environ., 34, 5183–5189, 2000.

Bonasoni, P., Cristofanelli, P., Calzolari, F., Bonafè, U., Evangelista, F., Van Dingenen, R., Colombo, T., and Balkanski, Y.: Aerosol and ozone correlation during the transport episodes of the summer-autumn 2000, period, Atmos. Chem. Phys. Discuss., this issue, 2002.

Bunz, H. and Dlugi R.: Numerical studies on the behaviour of aerosols in smog chambers J. Aerosol Sci. 22, 441–465, 1991.

Bunz H., Koyro, M., Möhler O., and Saathoff, H.: Redistribution of NH₄NO₃ within a system of (NH₄)₂SO₄- and NH₄NO₃-particles; Part 1: Modeling J. Aerosol Sci. 26, S465–S466, 1995.

Dentener, F. J. and Crutzen P. J.: Reactions of N₂O₅ on tropospheric aerosols: impact on the global distributions of NO_x, O₃, and OH, J. Geophys. Res., 98, 7149–7163, 1993.

Dentener, F. J., Carmichael, G. R., Zhang, Y., Lelieveld, J., and Crutzen P. J.: Role of mineral aerosol as a reactive surface in the global troposphere, J. Geophys. Res., 101, 22 869–22 889, 1996.

Fehsenfeld, F. C., Huey, L. G., Sueper, D. T., Norton, R. B., Williams, E. J., Eisele, F. L., Mauldin, III, R. L., and Tanner, D. J.: Ground-based intercomparison of nitric acid measurement techniques, J. Geophys. Res., 103, 3343–3353, 1998.

Fischer, H., Kormann, R., Klüpfel, T., Gurk, Ch., Königstedt, R., Parchatka, U., Mühle, J., Rhee, T. S., Brenninkmeijer, C. A. M., Bonasoni, P., and Stohl, A.: Ozone production and trace gas correlations during the June 2000 MINATROC intensive measurement campaign at Mt. Cimone, Atmos. Chem. Phys. Discuss., this issue, 2002.

Fonner, D. and Ganor, E.: The chemical and mineralogical composition of some urban atmospheric aerosols in Israel, Atmos. Environ., 26B, 126–133, 1992.

**Atmospheric
measurements of
gas-phase HNO₃
and SO₂**

M. Hanke et al.

Title Page

Abstract

Introduction

Conclusions

References

Tables

Figures

◀

▶

◀

▶

Back

Close

Full Screen / Esc

Print Version

Interactive Discussion

Furutani, H. and Akimoto, H.: Development and characterization of fast measurement system for gasphase nitric acid with a chemical ionization mass spectrometer in the marine boundary layer, *J. Geophys. Res.*, 107, 10.101029/2000JD000269, 2002.

Galy-Lacaux, C. and Modi, A. I.: Precipitation chemistry in the Sahelian savanna of Niger, Africa, *J. Atmos. Chem.*, 30, 319–343, 1998.

Gobbi, G. P., Barnaba, F., Van Dingenen, R., Putaud, J.-P., Mircea, M., and Facchini, M. C.: Lidar and in situ observations of continental and Saharan aerosol: Closure analysis of particles optical and physical properties, *Atmos. Chem. Phys. Discuss.*, this issue, 2002.

Goldan, P. D., Kuster, W. C., Albritton, D. L., Fehsenfeld, F. C., Connell, P. S., Norton, R. B., and Heubert, B. J.: Calibration and tests of the filter-collection method for measuring clean-air ambient levels of nitric acid, *Atmos. Environ.*, 15, 1081–1085, 1984.

Goodman, A. L., Underwood, G. M., and Grassian, V. H.: A laboratory study of the heterogeneous reaction of nitric acid on calcium carbonate particles, *J. Geophys. Res.*, 105, 29 053–29 064, 2000.

Gregory, G. L., Hoell, J. M., Huebert, B. J., Van Barmer, S. E., Lebel, P. J., Vay, S. A., Marinaro, R. M., Schiff, H. I., Hastlie, D. A., Mackay, G. I., and Karecki, D. R.: An intercomparison of airborne nitric acid measurements, *J. Geophys. Res.*, 95, 10 089–11 102, 1990.

Gregory, G. L., Davis, D. D., Beltz, N., Bandy, A. R., Ferek, R. J., and Thornton, D. C.: An intercomparison of aircraft instrumentation for tropospheric measurements of sulfur dioxide, *J. Geophys. Res.*, 98, 23 325–23 352, 1993.

Guimbaud, C., Labonette, D., Catoire, V., and Thomas, R.: High pressure flowing afterglow setup validated by the study of the CO₃ + HNO₃ reaction, *Int. J. Mass Spec.*, 178, 161–171, 1998.

Hanke, M., Uecker, J., Reiner, T., and Arnold, F.: Atmospheric peroxy radicals: ROXMAS, a new mass-septrometric methodology for speciated measurements of HO₂ and ΣRO₂ and first results, *Int. J. of Mass Spec.*, 213, 91–99, 2002.

Harnisch, F. and Crowley, J. N.: Heterogeneous reactivity of gaseous nitric acid on Al₂O₃, CaCO₃ and atmospheric dust samples: a Knudsen reactor study, *J. Phys. Chem.*, in press, 2001.

Harnisch F. and Crowley, J. N.: The influence of mineral dust on O₃, NO_x and NO_y: a laboratory study, *Proceedings of the 27th General Assembly of the European Geophysical Society*, 21–26 April 2002, Nice, France, *Geophysical Research Abstract*, Vol. 4, 2002.

Huey, L. G., Dunlea, E. J., Lovejoy, E. R., Hanson, D. R., Norton, R. B., Fehsenfeld, F. C., and

**Atmospheric
measurements of
gas-phase HNO₃
and SO₂**M. Hanke et al.

[Title Page](#)[Abstract](#)[Introduction](#)[Conclusions](#)[References](#)[Tables](#)[Figures](#)[⏪](#)[⏩](#)[◀](#)[▶](#)[Back](#)[Close](#)[Full Screen / Esc](#)[Print Version](#)[Interactive Discussion](#)

Howard, C. J.: Fast response measurements of HNO₃ in air with a chemical ionisation mass spectrometer, *J. Geophys. Res.*, 103, 3355–3360, 1998.

Hunton, D. E., Ballenthin, J. O., Borghetti, J. F., Federico, G. S., Miller, T. M., Thorn, W. F., Viggiano, A. A., Anderson, B. E., Cofer, III, W. R., McDougal, D. S., and Wey, C. C.: Chemical ionization mass spectrometric measurements of SO₂ emissions from jet engines and test chamber operations, *J. Geophys. Res.*, 105, 26 841–26 855, 2000.

IPCC 2001: Houghton, J. T., Ding, Y., Griggs, D. J., Noguer, M., van der Linden, P. J., Dai, X., Maskell, K., and Johnson, C. A. E.: IPCC, Climate Change 2001, Cambridge Univ. Press, 2001

Kley, P., Drummond, J. W., McFarland, M., and Liu, S. C.: Tropospheric profiles of NO_x, *J. Geophys. Res.*, 86, 3153–3161, 1981.

Knop, G. and Arnold, F.: Nitric acid vapor measurements in the troposphere and lower stratosphere by chemical ionisation mass spectrometry, *Planet. Space Sci.*, 33, 983–986, 1985.

Knop, G. and Arnold, F.: Stratospheric trace gas detection using a new balloon-borne ACIMS method: Acetonitrile, acetone, and nitric acid, *Geophys. Res. Lett.*, 14, 1262–1265, 1987.

Kondo, Y., Koike, M., Kawakami, S., Singh, H. B., Nakajima, H., Gregory, G. L., Blake, D. R., Sachse, G. W., Merrill, J. T., and Newell, R. E.: Profiles and partitioning of reactive nitrogen over the Pacific Ocean in winter and early spring, *J. Geophys. Res.*, 102, 28 663–28 671, 1997.

Liu, S. C., McFarland, M., Kley, D., Fafiriou, O., and Hübler, G.: Tropospheric NO_x and O₃ budgets in the equatorial Pacific, *J. Geophys. Res.*, 88, 1360–1368, 1983.

Liu, S. C., Trainer, M., Fehsenfeld, F. C., Parrish, D. D., Williams, E. J., Fahey, D. W., Hübler, G., and Murphy, P. C.: Ozone production in the rural troposphere and the implications for regional and global ozone distributions, *J. Geophys. Res.*, 92, 4191–4207, 1987.

Luther, III, G. W. and Stecher, III, H. A.: Preface, historical background, *J. Geophys. Res.*, 102, 16 215–16 217, 1997.

Mauldin, III, R. L., Tanner, D. J., and Eisele, F. L.: A new chemical ionization mass spectrometer technique for the fast measurement of gas-phase nitric acid in the atmosphere, *J. Geophys. Res.*, 103, 3361–3367, 1998.

Miller, T. M., Ballenthin, J. O., Meads, R. F., Hunton, D. E., Thorn, W. F., Viggiano, A. A., Kondo, Y., Koike, M., and Zhao, Y.: Chemical ionization mass spectrometer technique for the measurement of HNO₃ in air traffic corridors in the upper troposphere during the SONEX campaign, *J. Geophys. Res.*, 105, 3701–3707, 2000.

**Atmospheric
measurements of
gas-phase HNO₃
and SO₂**

M. Hanke et al.

Title Page

Abstract

Introduction

Conclusions

References

Tables

Figures

◀

▶

◀

▶

Back

Close

Full Screen / Esc

Print Version

Interactive Discussion

- Moehler, O. and Arnold, F.: Flow reactor and triple quadrupole mass spectrometer investigations of negative ion reactions involving nitric acid: Implications for atmospheric HNO₃ detection by Chemical Ionization Mass Spectrometry, *J. Atmos. Chem.*, 13, 33–61, 1991.
- Moehler, O., Reiner, T. and Arnold, F.: The formation of SO₅⁻ by gas phase ion-molecule reactions, *J. Chem., Phys.*, 97, 8233–8239, 1992.
- Moehler, O., Reiner, T., and Arnold, F.: A novel aircraft-based tandem MS for atmospheric ion and trace gas measurements, *Rev. Sci. Instr.*, 64, 1199–1207, 1993.
- Neuman, J. A., Huey, L. G., Ryerson, T. B., and Fahey, D. W.: Study of inlet materials for sampling atmospheric nitric acid, *Environ. Sci. Technol.*, 33, 1133–1136, 1999.
- Papenbrock, T. H. and Stuhl, F.: A laser-photolysis fragment-fluorescence (LPFF) method for the detection of gaseous nitric acid in ambient air, *J. Atmos. Chem.*, 10, 451–469, 1990.
- Parrish, D. D., Norton, R. B., Bollinger, M. J., Liu, S. C., Murphy P. C., Albritton, D. L., Fehsenfeld, F. C., and Huebert, B. J.: Measurements of HNO₃ and NO₃⁻ particulates at a rural site in the Colorado mountains, *J. Geophys. Res.*, 91, 5379–5393, 1986.
- Parrish, D. D. and Fehsenfeld, F. C.: Methods for gas-phase measurements of ozone, ozone precursors, and aerosol precursors, *Atmos. Environ.*, 34, 1921–1957, 2000.
- Phadnis, M. J. and Carmichael, G. R.: Numerical investigations of the influence of mineral dust on the tropospheric chemistry of East Asia, *J. Atmos. Chem.*, 36, 285–323, 2000.
- Putaud, J.-P., van Dingenen, R., Dell'Acqua, A., Matta, E., Decesari, S., Fachini, M. C., and Fuzzi, S.: Size-segregated aerosol mass closure and chemical composition in Monte Cimone (I) during Minatroc, *Atmos. Chem. Phys. Discuss.*, this issue, 2002.
- Reiner, T., Sprung, D., Jost, C., Gabriel, R., Mayol-Bracero, O. L., Andrea, M. O., Campos, T. L., and Shetter, R. E.: Chemical characterization of pollution layers over the tropical Indian Ocean: Signatures of emissions from biomass and fossil fuel burning, *J. Geophys. Res.*, 106, 28 497–28 510, 2001.
- Ryerson, T. B., Huey, L. G., Knapp, K., Neuman, J. A., Parrish, D. D., Sueper, D. T., and Fehsenfeld, F. C.: Design and initial characterization of an inlet for gas-phase NO_y measurements from aircraft, *J. Geophys. Res.*, 104, 5483–5492, 1999.
- Saathoff, H., Bunz, H., Möhler, O., and Schöck, W.: Redistribution of NH₄NO₃ within a system of (NH₄)₂SO₄- and NH₄NO₃-particles; Part 2: Experimental *J. Aerosol Sci.* 26, S551–S552, 1995.
- Schneider, J., Buerger, V., Droste-Franke, B., Grimm, F., Kirchner, G., Klemm, M., Stilp, T., Wohlfrom, K.-H., Arnold, F., Siegmund, P., and van Velthoven, P. F. J.: Nitric acid in the upper

**Atmospheric
measurements of
gas-phase HNO₃
and SO₂**M. Hanke et al.

[Title Page](#)[Abstract](#)[Introduction](#)[Conclusions](#)[References](#)[Tables](#)[Figures](#)[◀](#)[▶](#)[◀](#)[▶](#)[Back](#)[Close](#)[Full Screen / Esc](#)[Print Version](#)[Interactive Discussion](#)

troposphere and lower stratosphere at midlatitudes: New results from aircraft-based mass spectrometric measurements, *J. Geophys. Res.*, 103, 25 337–25 343, 1998.

Seeley, J. V., Morris, R. A., and Viggiano, A. A.: Rate constants for the reaction of CO₃⁻ (H₂O)_{n=0-5} + SO₂: Implications for CIMS detection of SO₂, *Geophys. Res. Lett.*, 24, 1379–1382, 1997.

Seinfeld, J. H. and Pandis, S. N.: *Atmospheric chemistry and physics*, John Wiley and Sons, New York, 1997.

Stecher, III, H. A., Luther, III, G. W., MacTaggart, D. L., Farwell, S. O., Crosley, D. R., Dorko, W. D., Goldan, P. D., Beltz, N., Krischke, U., Luke, W. T., Thornton, D. C., Talbot, R. W., Lefer, B. L., Scheuer, E. M., Benner, R. L., Wu, J., Saltzman, E. S., Gallagher, M. S., and Ferek, R. J.: Results of the gas-phase sulfur intercomparison experiment (GAISE): overview of experimental setup, results and general conclusions, *J. Geophys. Res.*, 102, 16 219–16 236, 1997.

Stohl, A., Wotawa, G., Seibert, P., and Kromp-Kolb, H.: Interpolation errors in wind fields as a function of spatial and temporal resolution and their impact on different types of kinematic trajectories, *J. Appl. Meteorology*, 34, 2149–2165, 1995.

Tabazadeh, A., Jacobson, M. Z., Singh, H. B., Toon, O. B., Lin, J. S., Chatfield, R. B., Thakur, A. N., Talbot, R. W., and Dibb, J. E.: Nitric acid scavenging by mineral and biomass burning aerosols, *Geophys. Res. Lett.*, 25, 4185–4188, 1998.

Talbot, R. W., Vijgen, A. S., and Harriss, R. C.: Measuring tropospheric HNO₃: Problems and prospects for nylon filter and mist chamber techniques, *J. Geophys. Res.*, 95, 7553–7561, 1990.

Tegen, I. and Fung, I.: Modeling of mineral dust in the atmosphere: Sources, transport, and optical thickness, *J. Geophys. Res.*, 99, 22 897–22 914, 1994.

Tegen, I. and Fung, I.: Contribution to the atmospheric mineral aerosol load from land surface modification, *J. Geophys. Res.*, 100, 18 707–18 726, 1995.

Ten Brink, H. M. and Veefkind J. P.: Humidity dependence of the light-scattering by ammonium nitrate, *J. Aerosol Sci.* 26, S553–S554, 1995.

Underwood, G. M., Song, C. H., Phadnis, M., Carmichael, G. R., and Grassian, V. H.: Heterogeneous reactions of NO₂ and HNO₃ on oxides and mineral dust: A combined laboratory and modelling study, *J. Geophys. Res.*, 106, 18 055–18 066, 2001.

van Dingenen, R., Putaud, J. P., Roselli, D., Dell'Acqua, A., Perrone, M. P., Bonasoni, P., and Facchini, M. C.: Comprehensive characterisation of physical and chemical properties of the

aerosol at Mt. Cimone, Atmos. Chem. Phys. Discuss., this issue, 2002.

Zhang, Y., Sunwoo, Y., Kotamarthi, V., and Carmichael, G. R.: Photochemical processes in the presence of dust: An evaluation of the impact of dust on particulate nitrate and ozone formation, J. Appl. Meteorology, 33, 813–824, 1994.

- 5 Zhang, Y., Chen, L. L., Carmichael, G. R., and Dentener, F.: The role of mineral aerosols in the tropospheric chemistry, in: Air Pollution Modeling and Its Applications XI, (Eds) Gryning and Schiermeier, Plenum Press, New York, 1996.

**Atmospheric
measurements of
gas-phase HNO₃
and SO₂**

M. Hanke et al.

Title Page

Abstract

Introduction

Conclusions

References

Tables

Figures

⏪

⏩

◀

▶

Back

Close

Full Screen / Esc

Print Version

Interactive Discussion

Table 1. Mean levels of gas-phase HNO_3 , SO_2 and O_3 for different air-mass classifications based on 3-D-back trajectories for the period 3 June – 5 July 2000. One-sigma standard deviations are given in parentheses

| Classification | Altitude | % | HNO_3/ppbv | SO_2/ppbv | O_3/ppbv |
|-----------------|----------|-----|----------------------------|---------------------------|--------------------------|
| Arctic | BL | NA | NA | NA | NA |
| | FT | 1% | 0.205 (0.035) | -0.002 (0.016) | 63 (9) |
| NW-Europe | BL | 9% | 1.206 (0.429) | 0.180 (0.064) | 65 (7) |
| | FT | 3% | 0.827 (0.208) | 0.168 (0.088) | 62 (4) |
| W-Europe | BL | 12% | 0.954 (0.700) | 0.205 (0.170) | 58 (10) |
| | FT | 12% | 0.817(0.371) | 0.356 (0.330) | 64 (5) |
| E-Europe | BL | 8% | 0.696 (0.271) | 0.517 (0.472) | 65 (8) |
| | FT | 9% | 0.720 (0.127) | 0.310 (0.267) | 56 (8) |
| Mediterranean | BL | 31% | 0.829 (0.439) | 0.387 (0.257) | 61 (7) |
| | FT | 5% | 0.607 (0.126) | 0.824 (1.417) | 60 (5) |
| Africa, no dust | BL | 5% | 0.800 (0.391) | 0.673 (0.582) | 68 (17) |
| | FT | NA | NA | NA | NA |
| Africa, dust | BL | 4% | 0.400 (0.287) | 0.515 (0.157) | 54 (4) |
| | FT | NA | NA | NA | NA |

Atmospheric measurements of gas-phase HNO_3 and SO_2

M. Hanke et al.

Title Page

Abstract

Introduction

Conclusions

References

Tables

Figures

◀

▶

◀

▶

Back

Close

Full Screen / Esc

Print Version

Interactive Discussion

Table 2. Statistics of HNO₃, SO₂ and O₃ measurements (30 min resolution) during upslope (08:00–22:00 LT =UTC + 2 h) and downslope (22:00–08:00 LT) conditions

| | HNO ₃ /pptv | SO ₂ /pptv | O ₃ /ppbv |
|-----------------|------------------------|-----------------------|----------------------|
| All data: | | | |
| Mean | 798 | 370 | 61 |
| Median | 798 | 245 | 61 |
| 1 σ -STD | 455 | 535 | 9 |
| Central 50% | 461–1071 | 120–495 | 56–66 |
| Range | 34–4636 | –14–8480 | 34–107 |
| Number | 798 | 920 | 1270 |
| 08:00–22:00 LT: | | | |
| Mean | 848 | 387 | 61 |
| Median | 777 | 254 | 59 |
| 1 σ -STD | 479 | 545 | 9 |
| Central 50% | 506–1130 | 130–524 | 55–64 |
| Range | 59–4636 | –14–8480 | 34–107 |
| Number | 525 | 613 | 793 |
| 22:00–08:00 LT: | | | |
| Mean | 703 | 337 | 63 |
| Median | 704 | 228 | 63 |
| 1 σ -STD | 389 | 514 | 8 |
| Central 50% | 367–971 | 112–421 | 58–68 |
| Range | 34–1957 | –13–7120 | 42–90 |
| Number | 273 | 307 | 477 |

Atmospheric measurements of gas-phase HNO₃ and SO₂

M. Hanke et al.

Title Page

Abstract

Introduction

Conclusions

References

Tables

Figures

◀

▶

◀

▶

Back

Close

Full Screen / Esc

Print Version

Interactive Discussion

Atmospheric measurements of gas-phase HNO₃ and SO₂

M. Hanke et al.

Table 3. Linear regressions results from Fig. 11

| | HNO ₃ | | SO ₂ | | O ₃ |
|---|--|---|--|---|---|
| Period of surface area increase of particles > 721 nm | HNO ₃ = (0.85 – 0.014 × S) ppbv with $r^2 = 0.67$ | = | SO ₂ = (0.72 – 0.0074 × S) ppbv with $r^2 = 0.41$ | = | O ₃ = (61.1 – 0.23 × S) ppbv with $r^2 = 0.52$ |
| Period of surface area decrease of particles > 721 nm | HNO ₃ = (0.83 – 0.015 × S) ppbv with $r^2 = 0.72$ | = | SO ₂ = (0.73 – 0.005 × S) ppbv with $r^2 = 0.47$ | = | O ₃ = (61.7 – 0.26 × S) ppbv with $r^2 = 0.64$ |

Title Page

Abstract

Introduction

Conclusions

References

Tables

Figures

⏪

⏩

◀

▶

Back

Close

Full Screen / Esc

Print Version

Interactive Discussion

Atmospheric measurements of gas-phase HNO₃ and SO₂

M. Hanke et al.

Table 4. Linear regressions results from Fig. 12

| | HNO ₃ | SO ₂ | O ₃ |
|---|---|--|---|
| Period of surface area increase of particles < 559 nm | HNO ₃ = (-0.32 + 0.005 × S) ppbv with $r^2 = 0.58$ | SO ₂ = (-0.04 + 0.004 × S) ppbv with $r^2 = 0.77$ | O ₃ = (37.7+0.12×S) ppbv with $r^2 = 0.87$ |
| Period of surface area decrease of particles < 559 nm | HNO ₃ = (-0.83 + 0.008 × S) ppbv with $r^2 = 0.76$ | SO ₂ = (-0.33 + 0.007 × S) ppbv with $r^2 = 0.73$ | O ₃ = (36.1-0.13×S) ppbv with $r^2 = 0.58$ |

Title Page

Abstract

Introduction

Conclusions

References

Tables

Figures

⏪

⏩

◀

▶

Back

Close

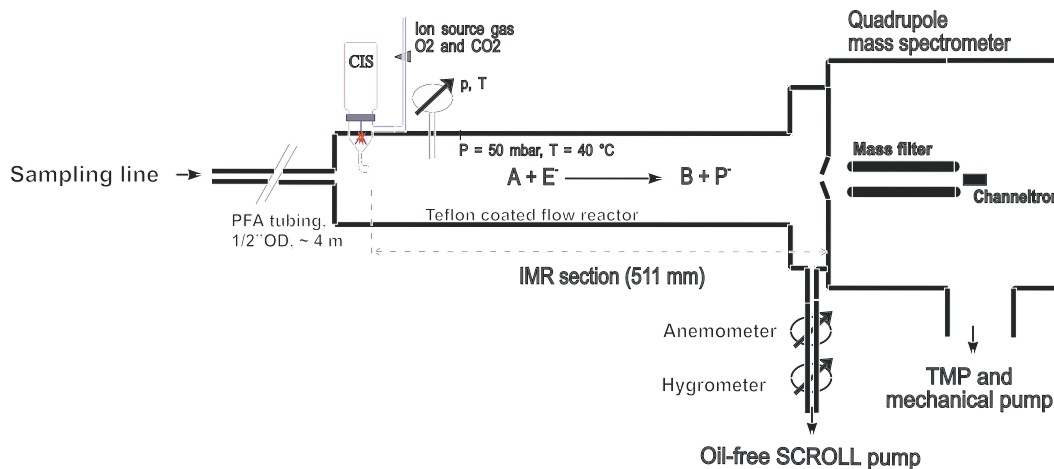
Full Screen / Esc

Print Version

Interactive Discussion

**Atmospheric
measurements of
gas-phase HNO_3
and SO_2**

M. Hanke et al.

**Fig. 1.** Schematic diagram of the CIMS apparatus (sampling line see Figs. 2 and 3).[Title Page](#)[Abstract](#)[Introduction](#)[Conclusions](#)[References](#)[Tables](#)[Figures](#)[◀](#)[▶](#)[◀](#)[▶](#)[Back](#)[Close](#)[Full Screen / Esc](#)[Print Version](#)[Interactive Discussion](#)

**Atmospheric
measurements of
gas-phase HNO_3
and SO_2**

M. Hanke et al.



Fig. 2. A measuring container housing the CIMS instrument was set up upwind from the CNR station with respect to the main wind direction (prevailing winds blow from SW) as indicated. A blow-up of the sampling line is shown in the right lower corner. In this way ambient air was sampled approximately 4.5 m above the ground and about 1 m above and in front of the container. The inlet pointed outwards towards the edge of the southern mountainside of Monte Cimone, i.e. in the main wind direction.

[Title Page](#)[Abstract](#)[Introduction](#)[Conclusions](#)[References](#)[Tables](#)[Figures](#)[I◀](#)[▶I](#)[◀](#)[▶](#)[Back](#)[Close](#)[Full Screen / Esc](#)[Print Version](#)[Interactive Discussion](#)

Atmospheric measurements of gas-phase HNO_3 and SO_2

M. Hanke et al.

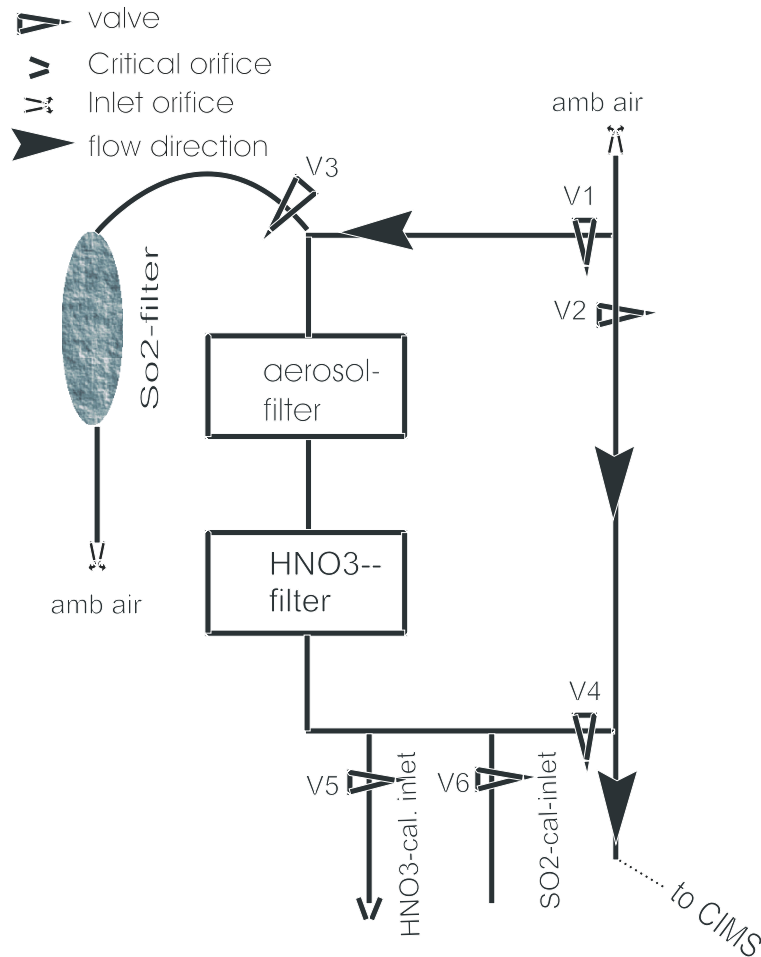


Fig. 3. Schematic diagram of the sampling-line system with filters and calibration-gas inlets for background and calibration measurements attached to the MPI-K CIMS instrument.

Title Page

Abstract

Introduction

Conclusions

References

Tables

Figures

◀

▶

◀

▶

Back

Close

Full Screen / Esc

Print Version

Interactive Discussion

Atmospheric
measurements of
gas-phase HNO_3
and SO_2

M. Hanke et al.

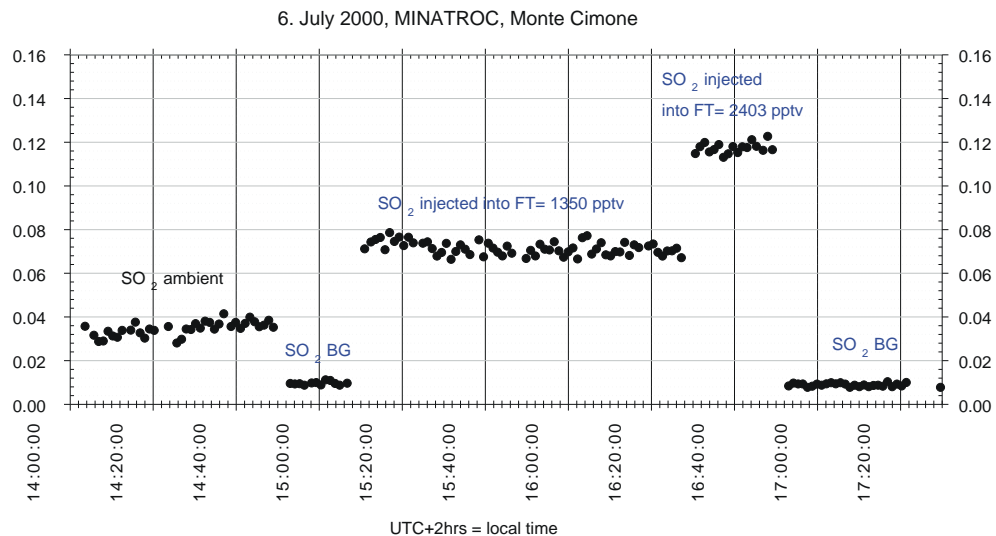


Fig. 4. Measured ratio of the ion count-rates from which the concentration of SO_2 is derived versus time during a sequence of background and calibration measurements during the field campaign on Monte Cimone. For more details see the text.

[Title Page](#)[Abstract](#)[Introduction](#)[Conclusions](#)[References](#)[Tables](#)[Figures](#)[⏪](#)[⏩](#)[◀](#)[▶](#)[Back](#)[Close](#)[Full Screen / Esc](#)[Print Version](#)[Interactive Discussion](#)

**Atmospheric
measurements of
gas-phase HNO_3
and SO_2**

M. Hanke et al.

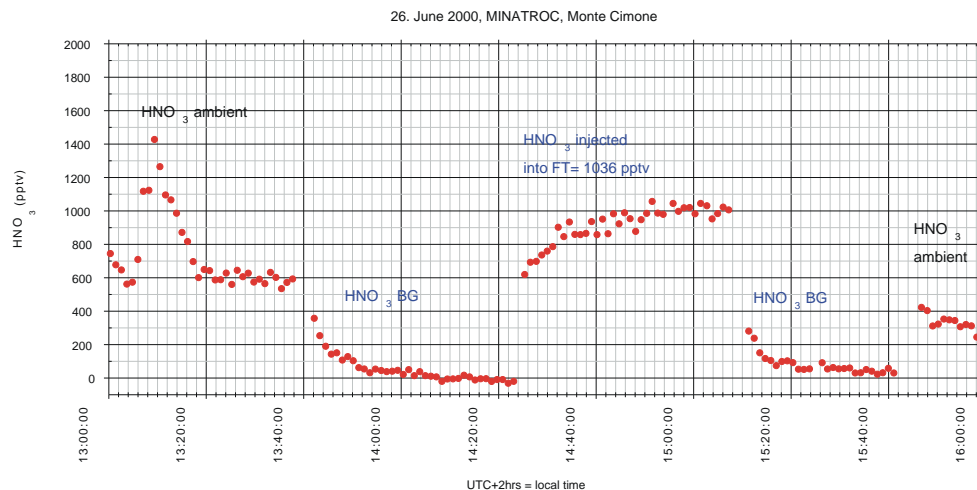


Fig. 5. Measured mixing ratio of HNO_3 versus time during a sequence of background and calibration measurements during the field campaign on Monte Cimone. For more details see the text.

Title Page

Abstract

Introduction

Conclusions

References

Tables

Figures

◀

▶

◀

▶

Back

Close

Full Screen / Esc

Print Version

Interactive Discussion

Atmospheric measurements of gas-phase HNO₃ and SO₂

M. Hanke et al.

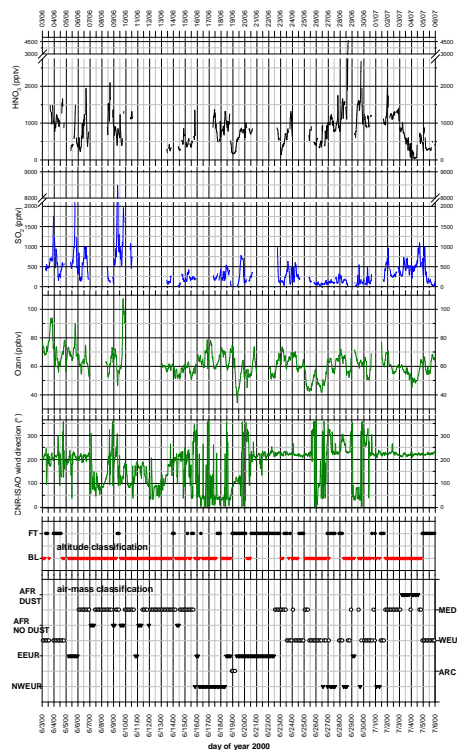


Fig. 6. Diurnal profiles of 30-min average values of HNO₃ (pptv) (upper panel), SO₂ (pptv) (second panel) and O₃ (ppbv) (third panel), and the wind direction (forth panel; CNR-ISAQ) measured on Monte Cimone (Italy, 2165 m above sea level) between 3 June and 6 July 2000. Two lowermost panels: air-mass classification according to altitude (FT = free troposphere and BL = boundary layer) and origin (ARC = arctic air, NWEUR = air from North Western Europe, WEUR = air from Western Europe, EEUR = air from Eastern Europe, MED = air from the Mediterranean basin, AFR NO DUST = air from Saharan Africa without dust and AFR DUST = air from Saharan Africa containing dust).

Title Page

Abstract

Introduction

Conclusions

References

Tables

Figures

◀

▶

◀

▶

Back

Close

Full Screen / Esc

Print Version

Interactive Discussion

Atmospheric
measurements of
gas-phase HNO_3
and SO_2

M. Hanke et al.

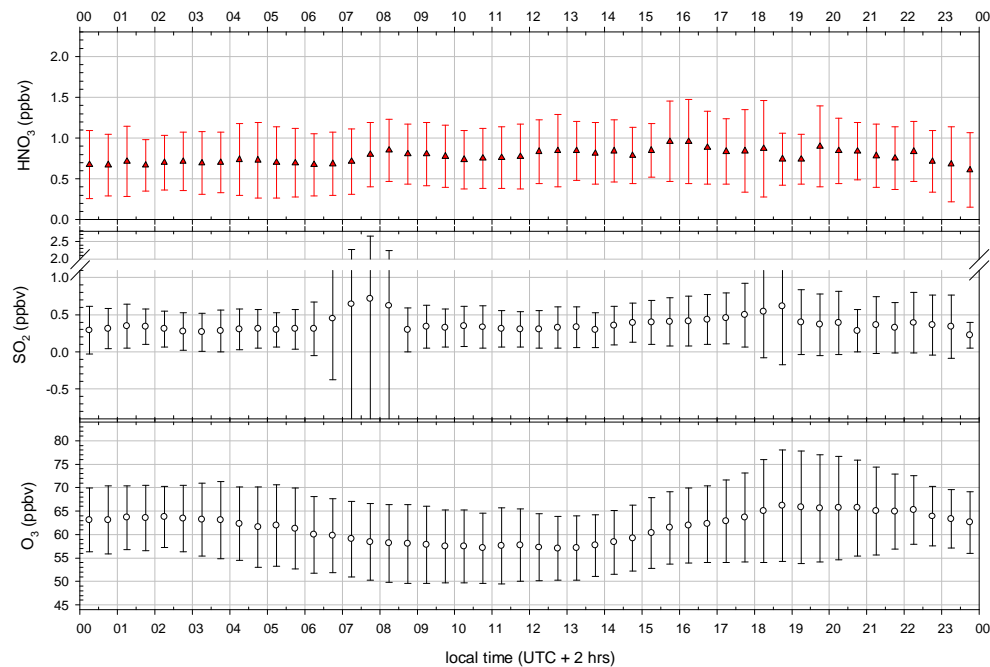


Fig. 7. Diurnal variation (mean $\pm 1\sigma$ -standard deviation) of the HNO_3 , SO_2 and O_3 measurements on Monte Cimone between 3 June and 6 July.

[Title Page](#)[Abstract](#)[Introduction](#)[Conclusions](#)[References](#)[Tables](#)[Figures](#)[◀](#)[▶](#)[◀](#)[▶](#)[Back](#)[Close](#)[Full Screen / Esc](#)[Print Version](#)[Interactive Discussion](#)

Atmospheric
measurements of
gas-phase HNO_3
and SO_2

M. Hanke et al.

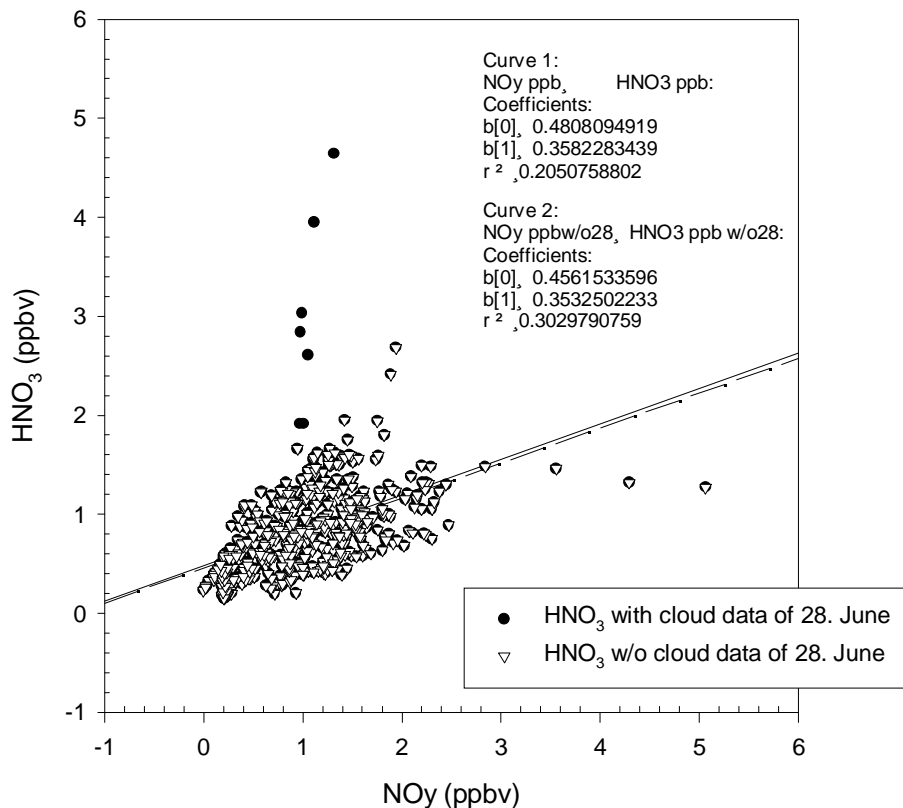


Fig. 8. Variations of HNO_3 versus NO_y (measured by MPI-CH, Mainz) based on 30-min averages. The solid symbols represent the data including the uncertain cloud data of 28 June and the white symbols those without these data. The lines show the linear regressions applied on the data.

[Title Page](#)[Abstract](#)[Introduction](#)[Conclusions](#)[References](#)[Tables](#)[Figures](#)[◀](#)[▶](#)[◀](#)[▶](#)[Back](#)[Close](#)[Full Screen / Esc](#)[Print Version](#)[Interactive Discussion](#)

Atmospheric
measurements of
gas-phase HNO_3
and SO_2

M. Hanke et al.

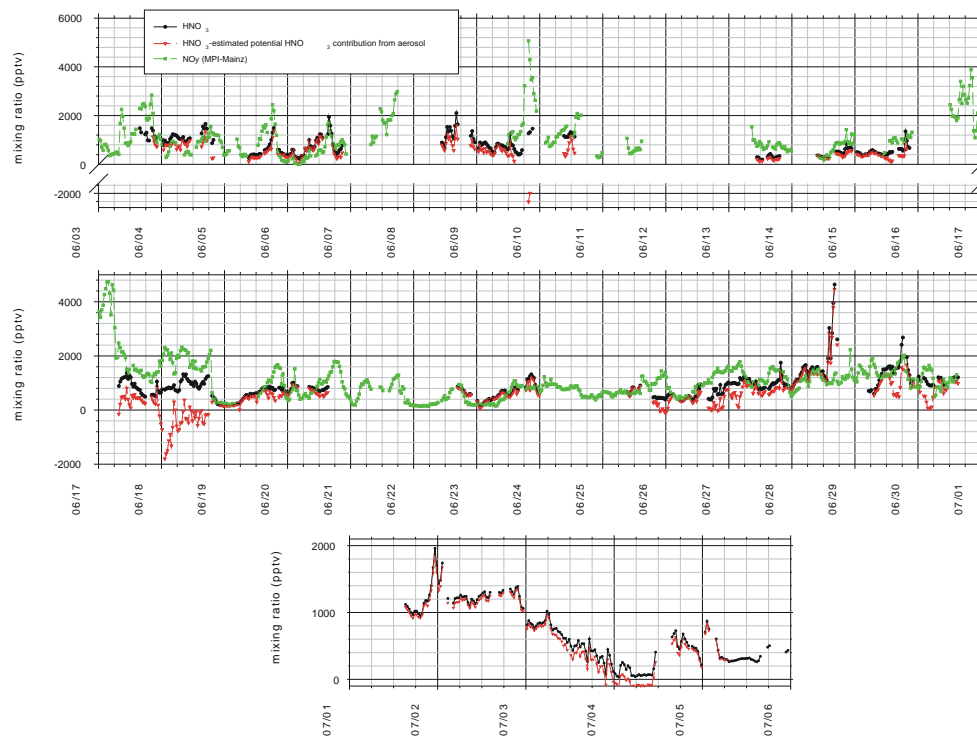


Fig. 9. Diurnal profiles of 30-min average values of atmospheric volume mixing ratios of the measured HNO_3 (CIMS MPI-K), HNO_3 from which an estimated potential aerosol contribution of HNO_3 resulting from possible evaporation of NH_4NO_3 aerosol has been subtracted, and NO_y measured by MPI-CH (Fischer et al., this issue). See discussion in text.

[Title Page](#)[Abstract](#)[Introduction](#)[Conclusions](#)[References](#)[Tables](#)[Figures](#)[◀](#)[▶](#)[◀](#)[▶](#)[Back](#)[Close](#)[Full Screen / Esc](#)[Print Version](#)[Interactive Discussion](#)

Atmospheric
measurements of
gas-phase HNO_3
and SO_2

M. Hanke et al.

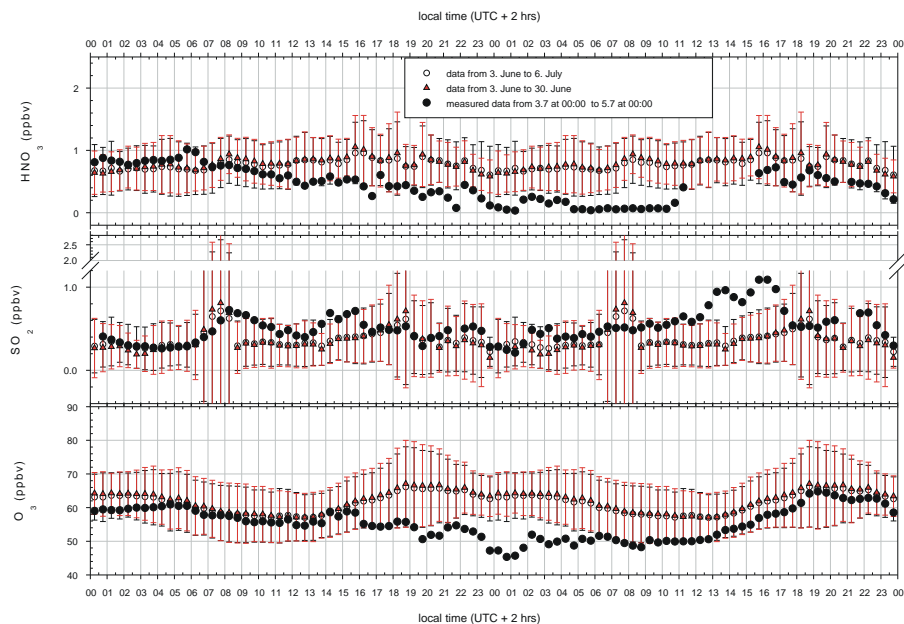


Fig. 10. Average bi-diurnal trends in HNO_3 , SO_2 and O_3 for the periods from 3 June to 6 July (including the dust event data), and 3 June to 30 June (outside the dust event) together with the same parameters measured during the dust event of 3–4 July 2000 at MTC.

Title Page

Abstract

Introduction

Conclusions

References

Tables

Figures

◀

▶

◀

▶

Back

Close

Full Screen / Esc

Print Version

Interactive Discussion

Atmospheric
measurements of
gas-phase HNO_3
and SO_2

M. Hanke et al.

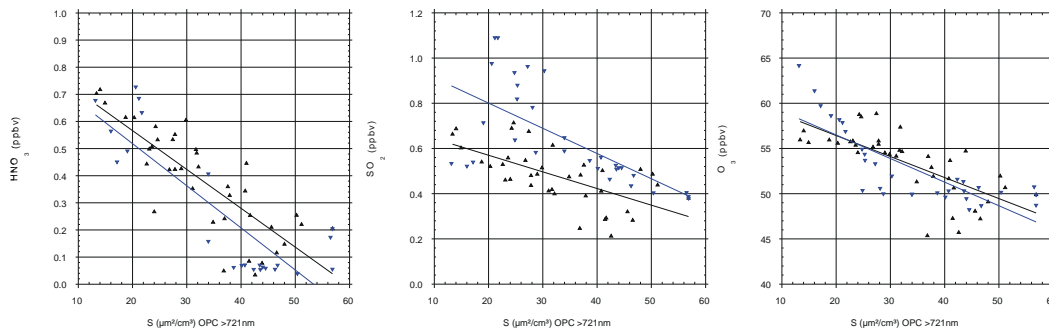


Fig. 11. Correlation plots of HNO_3 , SO_2 and O_3 versus the integrated surface area concentration for particles > 721 nm (S) measured with DMA/OPC (van Dingenen et al., this issue). It is distinguished between increasing surface area of the coarse particles between 08:45 LT 3 July and 03:45 LT 4 July (black symbols) and decreasing surface area between 04:45 LT 4 July and 18:45 LT 4 July (blue symbols). The lines represent regression lines.

[Title Page](#)[Abstract](#)[Introduction](#)[Conclusions](#)[References](#)[Tables](#)[Figures](#)[◀](#)[▶](#)[◀](#)[▶](#)[Back](#)[Close](#)[Full Screen / Esc](#)[Print Version](#)[Interactive Discussion](#)

Atmospheric
measurements of
gas-phase HNO_3
and SO_2

M. Hanke et al.

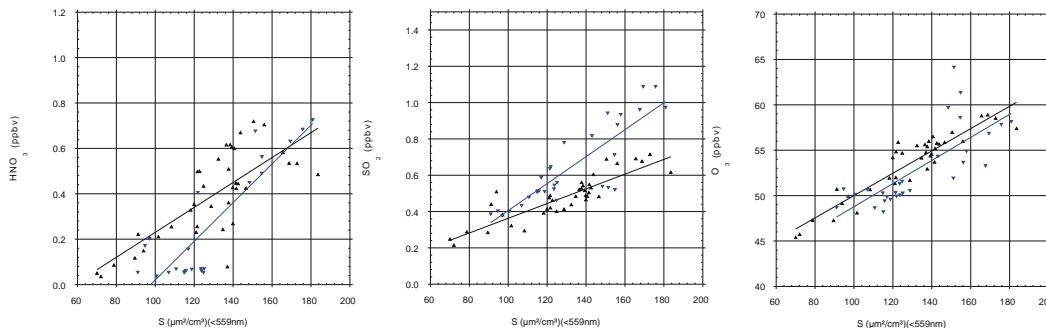


Fig. 12. Correlation plots of HNO_3 , SO_2 and O_3 versus the integrated surface area concentration for particles < 559 nm (S) measured with DMA/OPC (van Dingenen et al., this issue). It is distinguished between increasing surface area of the fine particles between 08:45 LT 3 July and 03:45 LT 4 July (black symbols) and decreasing surface area between 04:45 LT 4 July and 18:45 LT 4 July (blue symbols). The lines represent regression lines.

[Title Page](#)[Abstract](#)[Introduction](#)[Conclusions](#)[References](#)[Tables](#)[Figures](#)[◀](#)[▶](#)[◀](#)[▶](#)[Back](#)[Close](#)[Full Screen / Esc](#)[Print Version](#)[Interactive Discussion](#)